Author Manuscript

Author Manuscript

Author Manuscript

Author Manuscript

HHS Public Access

Author manuscript

Nat Rev Methods Primers. Author manuscript; available in PMC 2023 February 06.

Published in final edited form as:

Nat Rev Methods Primers. 2022 ; 2: . doi:10.1038/s43586-022-00162-2.

Optical coherence tomography

B.E. Bouma[*,1,2,3], **J.F. de Boer**[4], **D. Huang**[5], **I.K. Jang**[3,6], **T. Yonetsu**[13], **C.L. Leggett**[7], **R. Leitgeb**[8], **D.D. Sampson**[9], **M. Suter**[3,10], **B. Vakoc**[1,3], **M. Villiger**[1,3], **M. Wojtkowski**[11,12]

[1]Wellman Center for Photomedicine, Massachusetts General Hospital, Boston, MA, USA

[2]Institute for Medical Engineering and Physics, Massachusetts Institute of Technology, Cambridge, MA, USA

[3]Harvard Medical School, Boston, MA, USA

[4]Department of Physics and Astronomy, Vrije Universiteit Amsterdam, Amsterdam, The Netherlands

[5]Casey Eye Institute, Oregon Health and Science University, Portland, OR, USA

[6]Cardiology Division, Massachusetts General Hospital, Boston, MA, USA

[7]Division of Gastroenterology and Hepatology, Mayo Clinic, Rochester, MN, USA

[8]Institute of Medical Physics, University of Vienna, Wien, Austria

[9]School of Physics and School of Biosciences and Medicine, University of Surrey, Guildford, United Kingdom

[10]Division of Pulmonary and Critical Care Medicine, Massachusetts General Hospital, Boston, MA, USA

[11]Institute of Physical Chemistry and International Center for Translational Eye Research, Institute of Physical Chemistry, Polish Academy of Sciences, Warsaw, Poland

[12]Faculty of Physics, Astronomy and Informatics, Nicolaus Copernicus University, Torun, Poland

[13]Department of Cardiovascular Medicine, Tokyo Medical and Dental University

Abstract

Optical coherence tomography (OCT) is a non-contact method for imaging the topological and internal microstructure of samples in three dimensions. OCT can be configured as a conventional microscope, as an ophthalmic scanner, or using endoscopes and small diameter catheters for accessing internal biological organs. In this Primer, we describe the principles underpinning the different instrument configurations that are tailored to distinct imaging applications and explain the origin of signal, based on light scattering and propagation. Although OCT has been used for imaging inanimate objects, we focus our discussion on biological and medical

[*]Corresponding author: bouma@mgh.harvard.edu.

Author contributions

Introduction (BEB), Experimentation (BEB, JFdB, RL, DS, BV, MV, MW), Results (BEB, JFdB, RL, DS, BV, MV, MW), Applications (BEB, DH, IKJ, TY, CLL, MS), Reproducibility and data deposition (All authors), Limitations and optimizations (All authors), Outlook (All authors).

Author Manuscript Author Manuscript Author Manuscript Author Manuscript

imaging. We examine the signal processing methods and algorithms that make OCT exquisitely sensitive to reflections as weak as just a few photons and that reveal functional information in addition to structure. Image processing, display and interpretation, which are all critical for effective biomedical imaging, are discussed in the context of specific applications. Finally, we consider image artifacts and limitations that commonly arise and reflect on future advances and opportunities.

Key terms:

interferometry; Fourier-domain; spectral-domain; frequency-domain; resolution; detection sensitivity; spectrometer; wavelength-swept laser; Polarimetry; Angiography; Elastography

Introduction

Optical coherence tomography (OCT), first demonstrated in 1991,[1] is an optical method for cross-sectional imaging with a resolution approaching that of histopathology and a depth of penetration of a few mm. OCT utilizes interferometry to measure light reflected from a sample, permitting depth ranging, the discrimination of singly-scattered from diffuse, multiply-scattered light, and providing a large, noise-free amplification through optical heterodyning. Successive reflectance profiles are repeatedly acquired while the illuminating beam is swept transversely across the sample, mapping out a two-dimensional area or three-dimensional volume. The compiled data is then used to construct and display an image. Although the limited depth of penetration precludes whole-body or transillumination imaging of human organs, OCT is unrivaled in imaging the transparent tissues of the anterior eye and retina and its compatibility with optical fiber delivery makes it uniquely suitable for imaging internal organs through minimally invasive, narrow diameter catheters and endoscopes.

The phenomenon of optical interference has been well known since the time of Robert Hooke and Isaac Newton and interferometric methods have been exploited in research since the pioneering work of Michelson earned the Nobel Prize in Physics in 1907. Fundamentally, an interferometer enables the measurement of the electric field cross-correlation between light reflected from a sample and a coherent reference. The cross-correlation measurement can be performed by scanning the delay or path length of the interferometer reference arm, by scanning the optical frequency of the light source, or by analyzing the interferometer output as a function of wavenumber using a spectrometer. In the 1980's, these principles were used to measure the reflectance profiles of one-dimensional waveguides with high resolution and extremely high sensitivity, essentially at the level of single-photon detection. These 1D techniques were known as optical coherence domain ranging[2] and optical frequency domain ranging[3]. Coherence domain ranging was subsequently utilized to measure the length of the human eye, from cornea to retina.[4] In the early 1990's, MIT investigators had the insight that by performing multiple reflectance range measurements while scanning the beam across a sample and by mapping the resulting reflectance data to a color lookup table, a cross-sectional image could be produced. This was first demonstrated for imaging the human eye.[1]

Author Manuscript Author Manuscript Author Manuscript Author Manuscript

As ophthalmic OCT work progressed, new approaches and capabilities were demonstrated, including polarimetry for measuring tissue birefringence,[5,6] Doppler angiography to visualize blood flow,[7] elastography to measure tissue biomechanical properties,[8] and optimized light sources that provided over an order of magnitude improvement in resolution.[9] The success of ophthalmic OCT was, in part, due to the high transparency of ocular tissues, the ability to stabilize a subjects head through mechanical rests and the eye itself using a guide fixation beam, and the direct access to the cornea by free-space optical beams. The application of OCT to more highly scattering biological tissues required several advances: longer wavelength light sources to reduce scattering,[10] higher speed to avoid motion artifacts,[11] and fiberoptic catheters and associated rotational scanners.[12] By 1997, the first endoscopic and intravascular OCT was demonstrated in a living rabbit.[13]

Although it was well known that interferometric ranging could be performed using delay, wavenumber or frequency as the cross-correlation coordinate, essentially all OCT work prior to the turn of the millennium was performed using “time-domain” ranging and scanning of the interferometer reference optical delay. In this instance, the system includes a broadband light source and a photodiode detector to register fringes as a function of time or delay. Because this approach detects light reflected from one depth in the sample at any one time, the detection sensitivity diminishes with increasing scan rate and imaging speeds above a few images per second were unrealistic. It was therefore a significant advance when, in 2003, theoretical analyses clearly demonstrated that frequency-domain and spectral-domain interferometry provided detection sensitivity gains greater than 20 dB and therefore high speed imaging was made possible.[14–16] Both spectral-domain and frequency-domain approaches require Fourier transformation in order to compute the sample reflectance profile or axial-scan and are jointly termed “Fourier-domain” OCT. A simple way to see the origin of the sensitivity advantage of Fourier-domain techniques is to contrast the fact that time-domain detection registers signal from a single depth point per time, essentially throwing away the light that is simultaneously returned from other depths. Fourier methods, by comparison, collect reflected light from all depth points in parallel. In the literature, frequency-domain OCT is referred to as “swept-source OCT” and “optical frequency domain imaging”; we will use the acronym fd-OCT in the remainder of this manuscript. We will use the acronym sd-OCT to refer to spectral-domain OCT. High speed frequency-domain and spectral-domain systems were demonstrated shortly after the 2003 theoretical analysis, yielding image rates of hundreds of images per second while preserving the resolution and overall quality of previous time-domain technology.[17–19]

With the development of essential component technologies, fd-OCT technology became a better fit to the requirements of endoscopic applications and imaging in highly scattering tissues; sd-OCT more naturally met the needs in ophthalmology and retinal imaging in particular. Although the underlying factors have shifted somewhat in later years, sd-OCT remains most prevalent in ophthalmic imaging and fd-OCT more common in endoscopic applications. Other specific attributes of the Fourier-domain approaches determine which is optimal for angiographic, polarimetric and elastographic imaging.

In ophthalmology, OCT has become a standard of care for retinal imaging since 2003[20] and it is routinely used to guide refractive and cataract surgeries. In cardiology, intravascular

Author Manuscript Author Manuscript Author Manuscript Author Manuscript

OCT is internationally available for guiding coronary stenting and is routinely used in research related to coronary artery disease and acute myocardial infarction.[21] In gastroenterology, endoscopic OCT provides the ability to comprehensively interrogate the esophagus for neoplastic change and intramucosal cancer.[22] Although endobronchial OCT is not yet commercially available, research studies have shown its ability to diagnose and monitor pulmonary disease.[23] In preclinical research, OCT is routinely used to image small animal tumor models to investigate features such as angiogenesis and the response to novel anti-angiogenic therapies.[24]

The field of OCT continues to evolve, expanding into new applications, and capitalizing on new instrument capabilities. In this Primer, we present the principles that underpin reflectance, polarimetric, angiographic, and elastographic imaging with OCT and describe special requirements in the most common biomedical imaging applications. In addition, we provide a discussion of the instrumentation, methods and applications of circular ranging OCT. Although nascent, this technology opens many new opportunities for OCT that require very high speed or arbitrary stand-off distance between the objective and sample or in cases where the sample topology is non-uniform. Prior to circular ranging, such applications were infeasible. Defining a topical focus necessarily results in the exclusion of other potentially interesting topics. We do not address OCT imaging of non-biological samples, extensions to high numerical aperture[25] and en face imaging,[26] and less-developed biomedical application fields (e.g., dental, urology, gynecology, voice/speech, orthopedics). Recently, there has been an interest in combining other imaging modalities with OCT. Such ‘multi-modality’ approaches[27,28] address deficiencies in individual technologies, but have been additive combinations and are not covered herein.

Experimentation

In this section, we introduce the core components of OCT systems and the primary signal and image processing methods prior to addressing specialized variations of the technology.

Experimental Configuration

Basic Setup—Regardless of the specific variety, the fundamental subsystems for all OCT instruments include a light source, an interferometer comprising reference and sample paths, a beam scanning mechanism to control the illumination of a sample, and an optical receiver coupled with signal and image processing (Fig. 1). In simplest form, an OCT system repeatedly measures the reflectance profile of a sample along the optical axis as the illuminating beam is transversely swept across the sample. Signal processing is used to compute reflectance and ranging data that is subsequently processed to produce cross-sectional or volumetric images. An important design objective, regardless of the type of OCT systems, is to ensure that shot noise, the unavoidable signal characteristic arising from the particle nature of light, will be the dominant noise term. Achieving this specification is vital, since it will permit the greatest depth of imaging penetration, the highest speed, and the greatest volume of sample imaging. Each of the sections below provide general considerations, specific to each major OCT subsystem.

Author Manuscript Author Manuscript Author Manuscript Author Manuscript

Light Source: Many different types of light sources have been used for OCT, but the most common are either superluminescent or laser. The most relevant general characteristics include the wavelength, spectral shape and extent, spatial coherence, power, and noise. Typically, the wavelength of OCT light sources is chosen for a particular application to balance contributions to attenuation from scattering and absorption. However, practical constraints have also been influential since achieving high performance with regard to other specifications is not possible at arbitrary wavelengths. Since resolution along the optical axis within the sample is proportional to the spectral width of the source, significant effort has been directed to the development of broadband light sources. The axial point-spread-function of OCT is fundamentally determined by the Fourier transform of the spectral distribution of the source, a well-behaved, and preferentially Gaussian spectral distribution is ideal. In addition to these temporal coherence attributes, the light source must additionally have a high spatial coherence in order to ensure optimal signal collection efficiency and compatibility with convenient single-mode optical fiber. In addition to the temporal and spatial coherence requirements, the light source must also have sufficient power, typically on the order of tens of milliwatts, and low relative intensity noise.

Interferometer: Most commonly, Michelson and Mach-Zehnder interferometer topologies are used in OCT.[29,30] Importantly, the interferometer must have a spectral bandwidth sufficient to support the full extent of the light source spectrum, a reference arm having an adjustable and stable delay, a dispersion that ideally matches that of the sample arm and a low polarization mode dispersion. Because of the inherent stability of optical fiber, nearly all OCT systems utilize interferometers that are implemented using single mode optical fiber, beam splitters, circulators, polarizers, and polarization controllers. Largely owing to demand by the telecommunications sector, these components are available with exceptional optical performance and low price.

Beam Scanning: The OCT instrument must also provide for light delivery to/from the sample. Inherent in this function is spatial focusing at the sample, which provides for transverse resolution, and transverse beam scanning, which underpins the acquisition of two- and three-dimensional images. Although novel strategies have been deployed to control the light distribution at the sample, each has inherent trade-offs between transverse resolution and depth of field, which determines the cross-sectional image size in OCT. For common systems, Gaussian focal distributions are applied, resulting in a quadratic dependence of the depth of field on the transverse resolution. Subsequent sections of this Primer will detail the configuration of patient interfaces and associated beam scanners for different clinical imaging roles.

Optical Receiver: The design of the receiver in an OCT system depends upon the specific variety, with units for spectral domain and frequency domain systems having dramatically different approaches. While in fd-OCT, the receiver relies on a single photo-diode per polarization state, sd-OCT requires a spectrometer and a one-dimensional array of detector elements. However, common considerations are determined in order to achieve high sensitivity, low-noise conversion of the optical interferometric signal into an electronic signal. Importantly, the use of interferometry inherently embodies heterodyning

Author Manuscript Author Manuscript Author Manuscript Author Manuscript

or homodyning in which the signal is the cross-correlation of the electric fields returned from the reference and sample paths. This provides noise-free gain equal in magnitude to the strength of the reference electric field, typically on the order of one million. Therefore, OCT receivers do not require high gain preamplifiers as are required in confocal or fluorescence imaging. Since OCT is fundamentally an interferometric technique, receivers may be prone to polarization fading, a phenomenon arising from a mismatch between the polarization states returning from the sample and reference paths. Although the polarization state of the reference can, in principle, be controlled to match the average state of light returning from the sample, many samples are birefringent and some systems comprise sample paths in which the polarization state varies rapidly in time. A simple solution to polarization fading is the use of polarization-diverse detection[5] wherein the receiver splits the light returning from the reference arm into two orthogonal polarization eigenstates and measures the interferogram of sample reflectance simultaneously in both states. By subsequently computing the sum of squared amplitudes of these signals, which vary as cosine and sine functions individually, a polarization-independent signal is determined.

Signal and image processing: Common to all OCT systems, the signal that is detected encodes spatial ranging information in an interferogram. Decoding the signal may be conveniently performed using a common sequence of signal processing steps, including Fourier transformation (Fig. 2). However, the Fourier relationship that underpins this signal processing relies on the conjugate relationship of wavenumber and distance and many systems do not sample the interferogram rigorously in constant intervals of wavenumber. An initial processing step must therefore be used to interpolate from the inherent sampling of the system into wavenumber space. Another common processing step is used to compensate for any mismatch in the dispersion of the reference and sample arms. This is typically accomplished based on a calibration that is performed during the construction of the system and, barring any major reconfigurations, remains fixed.

Although the objective of all OCT systems is to render an accurate geometric representation of the physical structure of samples, interferometry fundamentally measures optical path delay, which is physical distance multiplied by index of refraction. A final signal processing step must therefore include an assumption or measurement of the index of refraction of the specific sample that is imaged. This measurement must include any portions of the sample that are in the beam path regardless of whether or not they are imaged.

Constructing two- and three-dimensional images in OCT is performed using algorithms that are commonly used in medical image formation and display. Image quality is dependent on the resolution, depth range, sensitivity and dynamic range of the instrument (Box 1).

Safety: The primary safety consideration in biomedical OCT is the possibility of photothermal damage, which depends upon the power density of light at the sample. The American National Standards Institute (ANSI) has determined maximum permissible exposure limits for visible and infrared light in the eye and skin and academic research has investigated photothermal damage in some other tissues. ANSI has also published methods for calculating exposure depending upon spot size, scanning dwell time, as well as specific

Author Manuscript Author Manuscript Author Manuscript Author Manuscript

characteristics of the light source. Owing to the very high detection sensitivity in OCT, high quality imaging is possible while remaining comfortably below exposure limits.

While ophthalmic OCT is a non-invasive procedure, imaging in the cardiovascular system, gastrointestinal tract, airways, and other internal organs is inherently invasive despite access through existing orifices and channels of the body. The overall evaluation of safety must therefore take into account risk of mechanically-induced trauma or infection from the intervention. Since OCT catheters and endoscopes may be fabricated using flexible, narrow diameter optical fiber, it has become routine to make biocompatible, disposable probes for human internal organ imaging.

OCT systems do not use ionizing radiation and permit electrical isolation from the patient, so these safety concerns are not relevant.

Spectral Domain OCT

In sd-OCT, the electric field cross-correlation is measured as a function of wavenumber. This is enabled using a light source having a broad, fixed spectrum, an interferometer with static path lengths, and an optical receiver including a spectrometer and an array detector.[31,32] This configuration permits a readout of the interference fringe pattern that is superimposed on the spectrum. To decode the interferogram and obtain a one-dimensional reflectance profile of the sample, a Fourier transform must be computed. Although the spectrometer and detector array in sd-OCT can provide shot-noise limited sensitivity, common detector arrays limit dynamic range. It turns out, however, that in the case of the eye, this parameter is not as demanding as in the case of imaging other organs due to the occurrence of small refractive index changes in the eye tissues. Only the central reflection from the cornea is problematic, which until now is simply neglected. There is also a relatively easy way to increase the dynamic range values by taking multiple measurements and averaging the data in postprocessing. Such an operation is only possible with a guaranteed high sensitivity of the method and is commonly used in commercial devices e.g. for imaging vitreous humor.

Since sd-OCT depends upon high performance detector arrays or line-scan cameras most instrument development has leveraged from mature silicon camera technology. As the spectral response of silicon is in the visible, extending to perhaps 1 μm, sd-OCT have characteristically operated in this wavelength range and therefore they have been most relevant to ophthalmic imaging where tissue scattering is very low. Additionally, spectroscopic detection relies on multiple detector elements that each integrate a weak signal at one corresponding wavelength. sd-OCT systems must therefore avoid sample motion during the integration to limit signal degradation. Specific artifacts arising from axial and transverse sample motion, which are specific to sd-OCT, have been analyzed in detail.[33]

Detection sensitivity roll off away from the depth in the sample that is matched to the length of the reference arm, is primarily governed by the finite resolution of the spectrometer and is given by:

Author Manuscript Author Manuscript Author Manuscript Author Manuscript

$$R(z) = \left(\frac{\sin\zeta}{\zeta}\right)^2 \cdot \exp\left[-\frac{w^2}{2\ln 2}\zeta^2\right],$$

where $\zeta = (\pi/2)*(z/z_{RD})$ denotes the depth relative to the maximum ranging depth, $z_{RD} = \lambda^2/(4\varsigma\lambda)$,[34] $\varsigma\lambda$ is the wavelength spacing per pixel, and $w = \delta\lambda/\varsigma\lambda$, where $\delta\lambda$ is the spectrometer resolution.[35] Typical values may be in the range of −6 dB roll off over 2 mm. The scanning speed in sd-OCT is simply determined by the readout rate of the line-scan camera with A-line rates of 100 kHz not uncommon.

Frequency Domain OCT

In fd-OCT, the signal is detected using a single-element photodiode and the interferometric fringe signal is encoded in frequency. This is enabled using a wavelength swept light source having a narrow instantaneous line width and a broad sweep range. As in sd-OCT, the interferometer in fd-OCT has static path lengths.[17] To decode the interferogram and obtain a one-dimensional reflectance profile of the sample, a Fourier transform must be computed. Frequency-domain OCT provides the same SNR advantage as sd-OCT.[14–16] The most striking advantage over sd-OCT is the ability to reach much larger ranging depths. This can be understood by examining the range of interferometer path length difference over which interference can be observed. In fd-OCT, this range is determined by the instantaneous linewidth of the light source.[17] It is straightforward to make wavelength swept lasers having line widths that support ranging depths of > 20 mm. Although this is an advantage over the range achievable in sd-OCT, its significance is application dependent.

The depth resolution in fd-OCT is determined by the range over which the light source sweeps. In practice, this spectral range is constrained by the physics of the laser gain medium and by phenomenon such as polarization mode dispersion, but sweep ranges on the order of one-tenth of the average wavelength are readily achieved. Typically, depth resolution in fd-OCT can easily be less than 10 μm but it is challenging to achieve a resolution below ~5 μm.

Significant advances in wavelength swept laser development have achieved sweep repetition rates from hundreds of kilohertz up to tens of megahertz,[36] resulting in data acquisition requirements of up to tens of giga-samples per second. A hurdle to achieve shot noise limited detection in fd-OCT is the narrow instantaneous line width of the source, which leads to a large relative intensity noise (RIN). However, the narrow instantaneous line width is needed for the large ranging depth. Balanced detection to suppress the common mode source noise (i.e., RIN) by 20–30 dB is required to reduce RIN to acceptable levels.[17] Commercial wavelength swept lasers typically do not provide linear or constant speed scanning. In order to facilitate data processing, especially the Fourier transform from wavenumber to depth, the raw frequency-encoded signal needs to be interpolated to points that are equally sampled in wavenumber. This can be accomplished by numerical interpolation in post processing, or directly by driving the digitization using a clock whose frequency is swept in synchrony with the laser sweep. This latter approach is known as k-clocking and is enabled using the output of a Mach-Zehnder interferometer with a path

Author Manuscript Author Manuscript Author Manuscript Author Manuscript

length difference of 4 times the maximum ranging depth.[37] The non-linear laser sweep velocity also requires optical and electronic paths to the data acquisition board to be of equal length in time. Dispersion imbalance in the interferometer can also be compensated numerically, as in sd-OCT.

Circular Ranging

When spectral-domain or frequency-domain OCT are used to interrogate a large spatial volume, a correspondingly large dataset is generated.[38–40] When coupled with the typical need for fast acquisition to avoid motion artifacts,[41,42] this result in an unrealistic need for data bandwidth and the electronics (e.g., optoelectronic receivers, digitizers, digital transfer busses, and processing engines) are commonly a bottleneck.

Circular-ranging (CR) architectures provide a means to interrogate large volumes with fewer measurements, allowing higher imaging speeds for a given electronic detection system.[41,43,44] This is achieved via signal compression in the optical domain. Rather than independently interrogating each voxel within a large three-dimensional volume (where one dimension is indexed by optical delay), CR pools the signals from multiple physical delays so that their sum can be captured by a single measurement. This pooling is performed according to a specific structure; equispaced delays are combined and the spacing between the delays is large enough to accommodate the typical depth of an OCT signal (1–2 mm). The resulting image is a circularly-wrapped representation of the sample that dedicates minimal if any data bandwidth to the empty space above and below the detectable signals (Figure 3a–c).

Optical frequency comb sources provide the physical basis for CR. Frequency combs have unique spectral and temporal properties that are leveraged in a broad set of scientific and metrology applications.[45,46] They are used in CR because they possess an inherent delay degeneracy; a frequency comb with a spectral comb line spacing of F is fundamentally unable to discriminate between optical delays spaced by $1/F$. When used as a ranging source, an equispaced delay pooling is achieved (Figure 3d,e).

Existing CR systems have relied on novel frequency comb laser sources that are constructed to generate each combline sequentially, resulting in a sequence of pulses with each pulse having a specific optical frequency. The earliest sources were based on existing continuously wavelength swept source architectures such as polygon-mirrors or tunable Fabry-Perot filters.[41] Fixed intracavity Fabry-Perot etalons were added to force combline outputs. These sources are simple to build, but they also retain the same speed and stability challenges of the platforms on which they are based.[43] Much faster CR sources have been enabled by a new laser architecture, stretched-pulse mode-locking (SPML).[47–49] These sources are based on electro-optic modulation with intracavity dispersive stretching and compression. They can operate at speeds exceeding 10 MHz. Through the use of continuously chirped fiber Bragg gratings (FBGS) as the positive and negative dispersive elements, they can also be made to be relatively compact and highly stable. More recently, wavelength-stepped frequency comb sources based on a phase-code mode-locked architecture have been demonstrated.[50] PCML uses electro-optic phase modulation

Author Manuscript Author Manuscript Author Manuscript Author Manuscript

and intracavity dispersion and has the advantage of providing output pulses that can be synchronized precisely to a master electronic clock.

Detection systems for CR are similar in design to those of fd-OCT, but of course they can operate at lower RF bandwidths than would be required for an analogous frequency-domain system. Of specific note is that complex fringe signals are required in CR, whereas it is sometimes used in frequency-domain but not required. Multiple approaches for complex fringe generation including polarization-based methods,[48] acousto-optic frequency shifters,[43] and lithium niobite phase modulators[44] have been used in CR.

Functional Imaging

Polarimetry—Polarization sensitive (PS) OCT employs two parallel, polarization-diverse detection channels.[5,51,52] The sample signal is split into two orthogonal polarization states, which independently interfere with identically orthogonally polarized reference signals in each channel. This can be accomplished using two cameras in sd-OCT systems[53] or using dual-balanced polarization-diverse detection in fd-OCT.[54] The relative phase difference and amplitude ratio between the two detection channels encodes the polarization state of the sample light, according to Jones formalism. Hence, PS-OCT measures the polarization state of backscattered light as a function of its path length traveled into the tissue. Many tissues, especially those with fibrillar architecture, are optically anisotropic and exhibit birefringence, causing a differential delay, or retardance, between light polarized parallel and orthogonal to the fibrillar tissue components. The path length-dependence of the detected polarization states enables tomographic reconstruction of tissue polarization properties, notably birefringence, that relate to the organization, orientation, and composition of tissue components. PS-OCT can furnish contrast between tissues that are indiscernible in conventional OCT tomograms and provides insight into the make-up and physical orientation of the tissue microstructure beyond the spatial resolution of OCT.

In order to unambiguously describe the polarization effect of round-trip transmission to a given sample depth, at least two distinct input polarization states are required. Algebraically, the Jones vectors measured in response to these input states enable recovery of the underlying Jones matrix.[55]This can be achieved either through sequential modulation of the source polarization state,[56] or by depth-multiplexing.[57,58] This measurement strategy enables the use of single-mode fiber- and catheter-based imaging systems, where the polarization state effectively incident onto the sample depends on the exact fiber configuration and is *a priori* unknown.

Alternatively, if the sample is assumed to be purely retarding, and considering that round-trip measurements constrain this retardation to be linear,[59] it is possible to employ a single circular input polarization state.[5,60] This requires careful control of the polarization state with fiber-based systems[61] or the use of polarization-maintaining fibers.[62,63] However, the achievable polarization sensitivity depends on the alignment of the polarization state with the tissue's optic axis, which can lead to the masking of sample birefringence in samples with a depth-dependent optic axis. Wavelength-dependent variation of the input polarization state can help mitigate this shortcoming.[64]

Author Manuscript Author Manuscript Author Manuscript Author Manuscript

Angiography—Blood flow is tightly linked to tissue nutrition, metabolism and as such to tissue health. Hence, the assessment of blood flow dynamics as well as the integrity of the vascular pathways are most important biomarkers in healthcare. Early on, researchers used the high sensitivity of OCT to detect small structural changes during a defined time interval for quantifying blood flow, termed Doppler OCT.[65,66] The blood flow signatures naturally outline the vascular tree, covering a large range of vessel types and sizes. Already a simply differential analysis of successively recorded tissue intensity images captures changes due to moving blood constituents. Such motion contrast forms the basis of OCT angiography (OCTA).[24,65,67,68] The advent of fast spectral and swept source OCT systems boosted the performance and quality of OCTA in terms of field-of-view, resolution, and suppression of motion artifacts and noise.[69,70] Since OCTA needs several images to extract the blood flow induced signatures from the bulk tissue, the recording is more time consuming than for standard OCT. Hence, involuntary motion adds to the motion contrast and needs to be properly suppressed, either by tracking systems, or by dedicated post-processing algorithms, or both. In general, the larger the time interval ΔT between recorded images to be analyzed, the higher the sensitivity of OCTA to slight blood flow changes, translating to higher contrast for smallest capillaries. This time dependence can be used to quantify blood flow based on the amount of signal decorrelation by analyzing images recorded at different interval times or by other advanced post-processing approaches.[71–73] Signal decorrelation is most easily assessed on the intensity or speckle level variance.[74,75] However, OCT exhibits also signal phase information which much faster decorrelates, in part, due to its cyclic nature.[76,77] On the other hand, phase-based OCTA is most sensitive to bulk motion and noise, such as trigger jitter. Best OCTA performance so far seems to be obtained by recurring to both domains and using the full complex OCT signal for decorrelation or motion analysis.[78–80]

Elastography—Elastography is the characterisation of the mechanical properties of human tissues, now in widespread clinical use based on ultrasonography and magnetic resonance imaging.[81] Optical imaging elastography has yet to progress to routine clinical application,[82] but important steps over the last five years have been made based on optical coherence tomography (OCT). OCT elastography, or optical coherence elastography (OCE), as it has come to be commonly known, was first advanced in 1998, and its progress has been comprehensively described.[83,84] Compared to elastography in current medical imaging, OCT has an advantage in superior resolution and a disadvantage in penetration. Its resolution often does not reach cellular scale, although near-cellular resolution has been demonstrated. Thus, OCE is often referred to as a “meso-scale” technique occupying the resolution range probing groups of cells – sitting between single cells and whole tissues.[82]

Elastography requires a stimulus and images the resulting changes. There exists a rich set of choices in methods based on stimulus parameters – the length scale relative to the imaging volume and time scale probed, whether harmonic or impulsive, and its source – intrinsic or extrinsic; contact or non-contact – OCE continues to mine this rich vein of novelty.[85,86] The most prominent methods today are based on quasi-static compression and shear/surface wave generation.

Author Manuscript Author Manuscript Author Manuscript Author Manuscript

In compressive OCE, a compressor operates between scans (usually B-scans) to capture images before and after compression. These images are compared to determine local axial strain from the slope of the displacement versus depth curve. Because OCT is capable of phase-sensitive detection (fractions of an interference fringe),[87] then high-dynamic range measurements are possible. Maximum displacements are set by speckle size or elastic limits of deformation to circa 10 μm and minimum resolvable displacements by phase noise from various sources to fractions of a nanometer.[87] Conversion of strain (a relative measure) to elastic (tangent) modulus (an absolute measure) has been demonstrated through addition of a compliant overlay used to sense stress.[88] Image acquisition rates to date have been limited by the volume scan rate of the OCT system and the need to oversample – 2 B-scans per location is a useful rule of thumb.

Shear and surface (Rayleigh) traveling waves can be generated by contact and non-contact means. Measurement of the shear (S-) wave velocity, c_s, typically in the 1–5 m/s range, can be used to estimate Young's modulus E from $E = 2\rho(1 + \upsilon)c_s^2$, where ρ is the density of the medium, and ν is Poisson's ratio. This simple relationship rarely holds in practice, not accounting for viscosity (most tissues are viscoelastic), nor for layer guidance (Lamb, Rayleigh-Lamb waves) and boundary effects. Shear wave velocity is most commonly determined from measurement of the transit time versus distance, presenting measurement challenges. Consider that the transit time for a 5 m/s wave to travel 3 mm across a 3 × 3-mm sample is 0.6 ms. To image the propagation with 100-μm transverse resolution, requires 30 orthogonal frames across the imaged region, requiring an OCT B-scan frame rate of 50 kHz. To maintain the same lateral resolution in the B-mode image (100 μm), an exceptional A-scan rate of 1.5 MHz is required, which, though demanding, can be achieved.[37] Recently, such "B-M mode" imaging has been joined by multi-excitation "M-B mode" imaging, requiring a lower A-scan rate, which appears promising.[86] Whether compression or shear wave imaging, accurate mechanical parameters require modeling to account for multiple effects, and this work is still in its early phases.[89,90]

Results

Image Reconstruction and Interpretation

Following the interpolation, dispersion compensation, and Fourier transformation described above, the resulting ensemble of axial reflectance profiles or A-lines are assembled to form an image (Figure 4) in which the two dimensional geometry is dictated by the specific scanning mechanism of the system (eg rectangular, circular, etc). Since the dynamic range of OCT is typically on the order of 50 dB, it is common to compute the logarithm of the signal and map this to a false color or grayscale lookup table for display. Three-dimensional OCT datasets are typically processed using widely available image processing software or routines that are available in packages such as MATLAB.

When novel imaging modalities are first applied for imaging specific biological tissues, suitable criteria for image interpretation must be identified and validated. In general, this process may involve the use of fabricated phantoms that mimic tissue but that have known structure, the use of cadaver tissue or surgical specimens, the use of animal models, or

Author Manuscript Author Manuscript Author Manuscript Author Manuscript

imaging *in vivo* with a comparison to an established medical imaging technology. When imaging biological tissues *ex vivo*, great care must be taken to avoid altering the optical properties of scattering and absorption, which may arise from dehydration or contamination. For example, when cadaver esophageal specimens are used, care must be taken to avoid gastric reflux that may arise at the time of death or after. Dehydration may be avoided by storing the samples on gauze that is saturated with isotonic saline. The temperature of samples must also be considered. While it is important to refrigerate samples to mitigate decomposition, it may be important in some specimens that they are returned to physiological temperature for imaging. This may be the case, for example, when imaging samples that contain lipids.

The use of animal models may be appropriate to determine and validate image interpretation criteria. Although the organ sizes of small animals are distinct from corresponding human organs, on the cellular level there may be sufficient similarities for imaging studies. Alternatively, large animal models may be required for imaging organs such as the arteries or airways. In either case, validation studies are typically conducted by imaging and subsequently harvesting tissues and performing histopathology while preserving spatial co-registration. For some clinical applications, it may be possible to conduct human clinical studies wherein imaging is performed followed by biopsy and histopathology. In some organs, however, such as the eye or the coronary arteries, biopsy is not possible. In these instances, validation of image interpretation criteria may be performed by comparing the novel image data with conventional medical imaging. In the case of OCT, it has been common to compare images with those from ultrasound since the spatial resolution is not too dissimilar. These comparisons may be quite challenging, however, as the image orientation and the physical origin of signal may be entirely distinct for the two modalities.

Spectral Domain and Frequency Domain OCT

Both Fourier domain techniques collect volumetric, or 3D, data by scanning successive dimensions in a sequential manner. First, information about the amplitude of scattered light as a function of depth (optical A-scan) is collected. Ensembles of A-scans recorded for different locations form a single cross-section and are called optical B-scans.[91] The set of B-scans, in turn, represents a volume. As with other tomographic techniques, there are many ways to visualize 3-D data in OCT. The most intuitive is to create projections in an arbitrary plane. Resolution in OCT, however, is not isotropic; the depth or axial resolution is typically 5 times higher than the transverse resolution.[92,93] Therefore, the preferred form of data visualization is a two-dimensional projection along the direction of light propagation and in one of the transverse directions.

In ophthalmic imaging, transverse scanning is performed using galvanometer-mounted mirrors to sample either the anterior eye or retina in cartesian coordinates (x-z or y-z). Circular scans (ϕ-z) are also frequently used to investigate retinal structure surrounding the fovea or optic nerve head or to assess retinal perfusion.[94,95] When using these scan patterns, the image is displayed in the acquired coordinates and no transformation is required.[96] In the analysis of the fundus or anterior chamber, a number of morphometric

Author Manuscript Author Manuscript Author Manuscript Author Manuscript

analyses have been proposed such as tissue layer thickness analyses, optic nerve disc architecture or corneal topography and pachymetry [97–103].

Circular cross-sectional scans in catheter-based OCT are produced by rotating the optical core of the catheter within the static sheath and acquiring data in circular coordinates (r,ϕ) and then transforming to cartesian coordinates for display. Three-dimensional data sets are registered by additionally performing “pull-back” scanning, withdrawing the core inside the sheath and acquiring a helical scan. The resulting data volumes may be visualized in 3D or manipulated to display arbitrary cross-sectional perspectives.[104] Quantitative analyses are performed using manually- or automated-segmentation.[105,106]

Circular Ranging

The display of CR datasets is a rapidly evolving topic. Presently, CR is being explored for surgical guidance where the real-time display of interpretable imagery is essential. The generation of compressed (i.e, circularly wrapped) three-dimensional datasets provide the input to a second stage of processing that either generates two-dimensional en face projections (Figure 3 x–y) or depth cross-sections (Figure 3 x–z) highlighting critical features, or that extracts features to annotate a second imaging modality, typically white-light camera images. Because CR is relatively new, existing work has utilized the former (projection to en face images), which can be implemented with relatively simpler algorithms. For both, functional approaches in OCT supporting clear, high-fidelity differentiation of tissue structures are critical. Polarization-based approaches are highly promising, and early applications have focused on the use of CR to identify tissues such as peripheral nerves with strong polarization signatures.[48]

Functional Imaging

Polarimetry—The cumulative round-trip measurements of PS-OCT are insensitive to polarization effects with circular eigenstates, preventing measurements of optical activity or circular dichroism.[59,107] A thin tissue section can be accurately modeled as the sequence of a linear retarder and linear diattenuator with identical eigenstates[108] (i.e., a homogeneous Jones matrix[109]). Using a single circular input polarization state provides measurements of cumulative retardance and optic axis orientation.[5] Fiber-based systems using two input states reconstruct cumulative retardance by referencing the depth-resolved polarization states to the tissue surface.[110] Cumulative measurements may be convenient for weakly scattering and retarding layers, such as the retina, but are difficult to interpret in tissues with multiple layers and distinct optic axis orientations. Recovering the local, depth-resolved scalar tissue birefringence requires matrix differentiation along depth, and can be achieved using Jones matrices,[55] geometric reasoning with Stokes vectors, [111] or Mueller matrix formalism.[112] To also recover the depth-resolved optic axis orientation, which relates to the eigenstates, and not just the eigenvalues of a given tissue layer, requires compensation for the transmission through the preceding tissue layers. [59,108,113] Many fiber-based systems furthermore suffer from a wavelength-dependence of the polarization states transmitted through fiber components. The differential delays caused by this polarization mode dispersion readily exceed those of the more subtle tissue effects,[114,115] and require specific processing strategies to enable meaningful

Author Manuscript Author Manuscript Author Manuscript Author Manuscript

measurements.[111,116] While PS-OCT only detects fully polarized, coherent states of light, incoherent spatial averaging of reconstructed Stokes vectors amounts to synthesizing a reduced degree of spatial coherence, and, hence, encompasses depolarization effects.[117] Depolarization quantifies the randomness of the detected polarization states within the spatial averaging window. It can serve to detect multiple scattering,[118] is pronounced in the retinal pigment epithelium[119] or in lipid-rich atherosclerotic plaques,[120] and can serve to detect exogenous contrast agents.[121] Examples of each of the above-mentioned polarimetric analyses applied to human intracoronary fd-OCT data are presented in Figure 5.

Angiography—The vascular tree is best appreciated in en face views. To this end, a full volume needs to be recorded and the motion contrast calculated as outlined in the Experimentation section. The presented enface view is calculated by projection (maximum intensity, average, standard deviation, etc.) along specific depth ranges (Figure 6a). Typical for OCTA are projection artifacts, i.e., motion signatures in the geometric shadow of vessels that need to be appropriately handled.[122] In case of the ocular fundus, one may distinguish various tissue plexi in depth. Capillary loss or neovascular growth as indicator of major retinal diseases such as proliferative diabetic retinopathy or wet age related macula degeneration can be easily spotted in OCTA enface maps.[68,123] For proper layer extraction along the natural shape of tissue, the retinal pigment epithelium may serve as perfect reference. In dermatology the vascular information provided by OCTA enhances the diagnostic capabilities for skin cancers (Figure 6b). The invasiveness or stage of tumor that is accompanied by characteristic chaotic neovascular growth is an important factor for clinical decisions regardless of anatomical tumor location (Figure 6c). In contrast to narrow-band endoscopic imaging, endoscopic OCTA has the advantage of deeper penetration as well as to provide volumetric vascular maps.[124,125] Current trends are to increase the field of view by increasing the recording speed, or by reducing the number of analyzed tomograms through efficient noise reduction. Vascular biomarkers include capillary density, fractal index, tortuosity, vessel diameter, or branching lengths.[24,126–128] Deep learning plays an increasingly important role for improving OCTA performance and for unleashing its full diagnostic potential.[129] Recent results encourage to use the eye as window to the brain by highlighting statistically relevant correlations between retinal vascular biomarkers and neurodegenerative diseases.[130]

Elastography—OCE has been explored at proof-of-principle level for many applications[83,84] but most published research has been directed towards the cornea, seeking to assess keratoconus and glaucoma,[86,131] including recently directly on human subjects.[132] In these applications, the transverse variation of mechanical properties is of primary interest and the display of elastography data is typically provided by projection onto the corneal surface or in a plane that is perpendicular to the optical axis. Similarly, for the investigation of retinal changes arising from macular degeneration, transverse projections are also most relevant.

Because biomechanical properties are known to vary during neoplastic changes, elastographic measurements may also be relevant in oncology. A recent study demonstrated that elastography measurements could help identify breast cancer tumor margins.[133] It

Author Manuscript Author Manuscript Author Manuscript Author Manuscript

is unclear whether en face projections or cross-sectional representation of biomechanical properties will be most relevant, however.

Other potentially impactful applications of elastography that are at earlier stages of development are cardiovascular assessment of vascular changes in atherosclerosis and as a general mesoscale method in mechanobiology and tissue engineering.[134–136]

Applications

Interface with biological sample

The interface between the imaging instrument and the sample is highly application-specific. Ophthalmic imaging, for example, typically requires non-contact delivery of light to the cornea through air. Cardiovascular imaging requires very narrow gauge (~ 0.8 mm), highly flexible, atraumatic catheters that are compatible with guidewires and that have lengths approaching 2 m. Endoscopic imaging of the esophagus is similar to intravascular imaging, but the diameter of the esophagus is much larger, requiring a mechanism for expanding the lumen and centering the imaging probe. In all of these applications, however, the common paradigm is that a focused beam illuminates the sample and a reflectance profile along the optical beam axis is measured. Such axial reflectance measurements, or A-lines, are repeatedly acquired while the beam is scanned transversely across the sample to generate an image. The depth- or axial-resolution of OCT is determined by interferometry and is typically less than 10 μm. Transverse resolution is determined by the focus of the beam on the sample. Since light is subject to diffraction, there is an important fundamental link between the tightness of a focus and the axial range over which the focus persists; focusing more tightly results in more rapid diffraction and a shallower depth of focus. Providing images having a depth range of a few mm therefore necessitates a compromise in transverse resolution. Typically, OCT is performed with a focal spot size of roughly 30 μm and this can easily be achieved with modest numerical aperture or f-number. Coupled with the fact that the spectral extent of the OCT light has a fractional bandwidth near 10%, the optical system that delivers light to the sample is relatively insensitive to aberrations and is simple and inexpensive. This characteristic is critical for applications where sterilization or safety dictate the use of disposal delivery optics.

Ophthalmic Imaging

Ophthalmology was the first clinical area where optical coherence tomography (OCT) was successfully applied.[137] Because the eye is highly transparent, the OCT scan beam can reach the back (fundus) of the eye with minimal loss to image the retina and optic nerve. Whereas fundus photography and scanning laser ophthalmoscopy provide 2-dimensional views of the fundus, OCT is inherently 3-dimensional. Thus *en face* OCT can be used to separately visualize many retinal and choroidal layers, and cross-sectional OCT can further pinpoint the depth of pathologic changes with micrometer precision. Because of these advantages, OCT had surpassed fundus photography and fluorescein angiography as the top Medicare reimbursed ophthalmic imaging procedure since 2003.[20] OCT angiography (OCTA) is a functional extension of OCT that was introduced as a commercial clinical device in 2014 and is gradually gaining adoption.

Author Manuscript Author Manuscript Author Manuscript Author Manuscript

OCT and OCTA are useful in the diagnosis and management of age-related macular degeneration (AMD), diabetic retinopathy, and glaucoma - the 3 leading causes of irreversible blindness. The most important new sight-saving therapy in the past two decades was intravitreal anti-vascular endothelial growth factor injections for exudative age-related macular degeneration (AMD) and diabetic macular edema. The primary indication for these injections is the accumulation of fluid inside or under the retina (Figure 8), as visualized by OCT.[138] OCT is also used to guide surgeries for macular hole and other sequelae of vitreoretinal traction syndrome.[139] OCTA is used to detect neovascularization (Figure 8) and ischemia in AMD, diabetic retinopathy, and other diseases.[140–142] Glaucoma and other optic nerve diseases cause thinning of the peripapillary retinal nerve fiber layer and macular ganglion cell complex, as well as loss of capillaries that supply these retinal layers.[143,144] These changes are now routinely detected by OCT and OCTA. This is particularly useful for the diagnosis and monitoring during the early stages of glaucoma, when timely treatment can be more effective in preventing significant visual impairment.[145]

OCT is also used to visualize and measure the anterior segment of the eye. Corneal tomography and topography are used to guide laser and surgical treatments.[146,147] Anterior chamber angle measurements are used to diagnose angle-closure glaucoma.[148] And biometric measurements of the cornea and lens are useful for selecting the intraocular lens implant in cataract surgery.[149]

Intravascular Imaging

In current practice, the gold standard for diagnosing coronary artery disease is the coronary angiogram. Coronary angiography is a “luminogram”, by which we look at changes not in the disease itself, but changes in the adjacent structure.[150] The development of intravascular imaging modalities has made a significant contribution both to the facilitation of percutaneous coronary intervention (PCI) and to a better understanding of *in vivo* vascular biology. Several meta-analyses demonstrated significant mortality reduction when PCI was guided by intravascular ultrasound (IVUS). Intravascular OCT was first demonstrated in human subjects in 2001[151] and criteria were developed for characterizing atherosclerosis,[152,153] monitoring stenting,[154] and identifying macrophages.[155] Compared to IVUS, OCT has 10-fold higher resolution and 40 times faster pull-back speed (shorter image acquisition time).[104] Although data on OCT-guided PCI is limited at present, there has been an explosion of studies using OCT to study coronary atherosclerosis.

Contemporary PCI is performed with a 6 or 7 Fr size guiding catheter, a 0.014 inches guidewire, and balloon / stent delivery systems. An intravascular OCT imaging catheter is composed of an optical fiber and lens within a transparent sheath which is advanced into the coronary artery over a guidewire.[156] The OCT catheter is placed in the distal portion of the culprit lesion to obtain the cross-sectional images of the artery, and blood is displaced from the lumen by injecting contrast medium for 3–4 seconds, during which the optical fiber is automatically pulled-back obtaining 180 frames of images per second (75mm in approximately 2 seconds).

As previously mentioned, OCT offers high resolution images of vascular structures. There are two clinical indications for OCT: facilitation of PCI and a diagnosis of underlying

Author Manuscript Author Manuscript Author Manuscript Author Manuscript

mechanism of ischemia or infarction with non-obstructive lesions. In the setting of PCI, information on plaque composition as well as the reference vessel size and the lesion length can be obtained by OCT. Based on this information, the optimal stent (size and length) is chosen and the stenting strategy (direct stenting vs. predilation, need for high pressure inflation using a non-compliant balloon, etc.) is developed (Figure 9A). However, in contrast to the body of data generated by IVUS-guided PCI, only several randomized studies have been carried out to evaluate the value of OCT-guided PCI to improve outcomes. ILUMIEN III: OPTIMIZE PCI study was a randomized controlled trial which compared the acute results of stent deployment and 30-day outcomes among OCT-guided, IVUS-guided, and angiography-guided PCI.[157] This study demonstrated comparable minimal stent cross-sectional area and similar adverse cardiac event rates between OCT-guided and IVUS-guided PCI, but less frequent intimal dissection or strut malapposition in OCT-guided PCI than in IVUS-guided PCI. The OPINION trial corroborated ILUMIEN III, showing an almost identical target vessel failure-free survival rate between OCT-guided PCI and IVUS-guided PCI, which lasted until 12 months.[158] The conclusion is that no study has convincingly demonstrated that OCT-guided PCI is better than IVUS-guided PCI. Another entity where OCT has a unique value is in myocardial infarction / ischemia with non-obstructive coronary artery disease,[159] which has been attributed to multiple causes such as small disruption of mild atherosclerotic plaque, coronary thrombosis, spontaneous coronary artery dissection, coronary spasm, or microvascular disease, in which OCT is a crucial tool to rule out a vascular origin along with cardiac magnetic resonance imaging. [160]

As mentioned above, convincing evidence showing that OCT-guided PCI improves patients' outcomes would be crucial for the future of OCT in cardiology. Another potential role of OCT is the identification of plaque erosion in patients with acute coronary syndromes (ACS). As the nature of plaque erosion is distinct from plaque rupture, the therapeutic strategy may need to be tailored based on the plaque phenotype. Indeed, the proof-of-concept EROSION study showed conservative management without stenting may be an option for patients with ACS caused by plaque erosion.[161] If the result of the EROSION study is replicated in randomized controlled trials, it may potentially change the management of millions of patients with ACS around the world annually.

Gastrointestinal Endoscopy

Gastrointestinal endoscopy is indicated in the evaluation of a variety of gastrointestinal symptoms and often used to screen patient populations at risk of certain gastrointestinal disorders and to perform surveillance and treatment of established disease. The diagnostic capability of gastrointestinal endoscopy is limited by visualization of mucosal surface morphology and vascular patterns and often requires tissue biopsies for histopathologic confirmation of disease. Advanced imaging modalities such as OCT[162] provide an 'optical biopsy' capable of enhancing real-time diagnosis and guiding treatment.

Esophagogastric Optical Coherence Tomography—Barrett's esophagus (BE), the metaplastic transformation of the normal squamous epithelium that lines the distal esophagus, is considered the precursor to esophageal adenocarcinoma and can undergo

Author Manuscript Author Manuscript Author Manuscript Author Manuscript

neoplastic progression through stepwise dysplastic changes. Random endoscopic biopsies are used to diagnose BE, but can lead to a missed diagnosis of dysplasia.[163] In this context, the application of OCT to BE surveillance aims to enhance the diagnostic yield of BE dysplasia and provide real-time diagnosis that can be used to guide treatment.[164] Early studies using a linear scanning OCT endoscopic probe (axial resolution 10 um, depth of imaging 2.5 mm)[29] describe features capable of distinguishing intestinal metaplasia from normal squamous epithelium and dysplastic BE including changes in the normal squamous layered architecture and differences in surface signal intensity and epithelial glandular architecture.[165,166] Subsequently, a next-generation fd-OCT system was designed specifically for BE surveillance using a balloon-based rotational imaging probe capable of volumetric imaging across 6 cm of the esophagus (Figure 9B) with an axial resolution of 7 μm, and an imaging depth 3 mm).[104] This instrument was commercialized under the Nvision NinePoint Medical Volumetric Laser Endomicroscopy (VLE) system.[167] The VLE system was capable of performing laser directed marking[168] of OCT abnormalities for targeted endoscopic biopsy and included a computer assisted OCT image interpretation software.[169] A multicenter study determined the feasibility of VLE for BE surveillance and was followed by refinement and incorporation of OCT diagnostic criteria for BE dysplasia.[22,170,171] The cross-sectional imaging capability of VLE makes it particularly useful in evaluating for Barrett's mucosa buried underneath squamous epithelium,[172,173] and for guiding BE endoscopic therapy.[174] Several studies have also demonstrated the utility of VLE in staging early-stage esophageal adenocarcinoma and squamous cell carcinoma. Further advancements in OCT techniques have included the application of deep learning for automated diagnosis, [174] and a tethered capsule capable of imaging the esophagus without white light endoscopy and conscious sedation.[175,176]

Small Bowel and Colorectal Optical Coherence Tomography—Accurate characterization of colorectal polyps during colonoscopy is associated with direct impact on clinical practice. Mucosal pit and crypt patterns that distinguish adenomatous from hyperplastic polyps can be visualized with endoscopic OCT and enhanced by en-face imaging.[177] Crohn's disease (CD) and ulcerative colitis are autoimmune inflammatory disorders of the gastrointestinal tract that can be distinguished by their clinical presentation including the presence of transmural inflammation. Disruption of the layered architecture of the colon wall can be observed with OCT and was found to be an accurate marker for transmural inflammation in CD.[178] Celiac disease is an autoimmune disorder that leads to villous atrophy of the small bowel from exposure to gluten in the diet. OCT and TCE have been used to visualize small bowel villi and measure degree of villous atrophy in patients with Celiac disease.[176,179]

Pancreaticobiliary Optical Coherence Tomography—Primary sclerosing cholangitis (PSC) is a progressive liver disease associated with inflammation and fibrosis of the intra and extrahepatic bile ducts. Endoscopic retrograde cholangiopancreatography (ERCP) in conjunction with adjunct imaging modalities is often required to distinguish between a benign PSC stricture and bile duct cancer. OCT imaging of the pancreaticobiliary ductal system is performed using ultrathin imaging probes capable of fitting through the ERCP instrument channel. First generation probes consisted of a rotating OCT catheter housed

Author Manuscript Author Manuscript Author Manuscript Author Manuscript

within a transparent sheath (1.2 and 2.4 mm diameter).[180] A second-generation low-profile (2.3 mm diameter) probe was developed for use with the NinePoint VLE system.[181] Several studies describe OCT morphological features associated with malignant biliary strictures including epithelial thickening, a hyperreflective surface and loss of inner wall layering.[182,183] Similarly, OCT features of lack of layered architecture and heterogenous backscattering have been used to describe malignancy associated with the main pancreatic duct.[184] The clinical diagnostic performance of OCT in the diagnosis of pancreaticobiliary pathology is an area of ongoing study.

Pulmonary Bronchoscopy

The detection, diagnosis and monitoring of pulmonary diseases is highly dependent on imaging. Computed tomography (CT) can detect and localize regions of abnormality but often lacks the necessary resolution and contrast for diagnosis. Tissue sampling for diagnosis either by minimally invasive endobronchial biopsy, or surgical biopsy can be associated with increased risks to the patient and is subject to sampling errors. The use of endobronchial OCT to address these limitations in pulmonary medicine has gained significant traction in recent years. Much of the work has been focused on the use of OCT for aiding in the detection and diagnosis of airway pathology, in monitoring disease progression over time, and in assessing the dynamic microstructure and function in vivo. Specific disease examples where OCT is making an impact include asthma and obstructive lung diseases, lung cancer, and more recently interstitial lung disease.

Obstructive lung disease—Airway remodeling is a characteristic feature of obstructive lung diseases including asthma and chronic obstructive pulmonary disease (COPD) and has been shown to be closely associated with disease severity.[185] While CT imaging is capable of assessing changes in airway wall thickness, it cannot discern individual layers of the airway wall or differentiate mucus from tissue. A number of studies have demonstrated that OCT can accurately identify and measure individual layers of the airway wall, with results validated against histology[23,186,187]. Studies have demonstrated the clinical potential of OCT to assess airway remodeling associated with pulmonary function decline. OCT measurements of airway wall thickness have been demonstrated to correlate with pulmonary lung function in smokers and individuals with COPD,[188,189] and OCT assessments of airway remodeling including epithelial thickening and mucosal buckling (a metric to assess bronchoconstriction) were found to correlate with a decrease in lung function in individuals with asthma (Figure 9C).[190]

Increased thickness of airway smooth muscle (ASM) through remodeling is a key feature of both COPD and asthma and contraction of the ASM resulting in bronchoconstriction promotes airway obstruction. By incorporating PS-OCT to measure the tissue birefringence, ASM can be accurately and reliably detected and quantified (Figure 9 C).[191] In addition, birefringence has been found to correlate to ASM force of contraction in limited studies providing crucial information not only on the amount of ASM but also its function.[191] A pilot study recently reported on the potential utility of PS-OCT for monitoring the response to therapeutic bronchial thermoplasty for the treatment of poorly controlled asthma and determining which patients are most likely to respond favorably to this treatment.[192]

Author Manuscript Author Manuscript Author Manuscript Author Manuscript

Lung Cancer—As with any malignancy, early diagnosis of lung cancer is critical to patient survival. While computed tomography (CT) has made significant strides in increasing early detection, diagnosis must be made on the microscopic level, typically with high-risk surgical biopsy or bronchoscopic biopsy, which has low diagnostic yields. The use of OCT for addressing this diagnostic gap has largely focused on biopsy guidance to increase diagnostic yields of the low risk bronchoscopic approaches. Following early feasibility studies that demonstrated the potential of OCT to detect neoplasia and early cancer in the airway wall [193–196] investigators focused on the development and clinical validation of image interpretation criteria.[23,197–199] The accuracy of OCT diagnosis of lung cancer has been reported in the range of 73.7–94.7% in a blinded review of OCT images from surgical resections.[199] Though future large scale clinical studies are clearly needed, these results suggest that intra-procedural OCT diagnosis may provide critical information to the treating physician in cases where diagnostic accuracy by traditional means remain unacceptably low.

Interstitial Lung Disease—More recently, investigators have explored the potential of OCT for aiding in the diagnosis of interstitial lung disease (ILD), particularly idiopathic pulmonary fibrosis (IPF), which is a fatal form of ILD with the worst prognosis. The diagnosis of IPF is challenging and often requires a multidisciplinary approach including radiographic and pathologic assessments. OCT has been shown to detect many of the pathologic features of ILD including the development of fibrosis and the presence of features such as honeycombing, cysts, and bronchiectasis, which are all necessary features for diagnosis (Figure 9C).[200] A clinical pilot study conducted in 27 ILD patients undergoing surgical biopsy demonstrated that OCT could accurately detect microscopic honeycombing and traction bronchiectasis that was not found on CT and that OCT could diagnose IPF with a sensitivity of 100% (95% CI: 75.8% - 100%) and specificity of 100% (95% CI: 79.6%−100%) when compared to the clinical diagnosis of IPF.[201] Though additional clinical research will be required, these early results indicate a promising future role for OCT in the clinical management of individuals with ILD.

Reproducibility and data deposition

DICOM®, which is recognized by the International Organization for Standardization as the ISO 12052 standard for archiving medical imaging and related data, has established standards for ophthalmic, cardiovascular, endoscopic and angiographic OCT image data. It appears, however, that most instrument manufacturers utilize proprietary data formats, which complicates efforts to standardize and disseminate image processing software. Similarly, no uniform standards have been adopted by system manufacturers for color or grayscale lookup tables. Since commercial systems only provide processed images rather than raw fringe data, this represents a major hurdle for standardization.

As previously discussed, the interferometer in OCT measures optical distances and calibration by the sample index of refraction is required to accurately portray the physical structure of the sample. Further complicating matters, the index of refraction is not homogeneous in most biological tissues and it can vary within individual OCT cross-sections. In applications where accurate distance measurements are required to guide

Author Manuscript Author Manuscript Author Manuscript Author Manuscript

intervention, as in the case of stent sizing in cardiovascular OCT, it is important to accurately measure the relevant index. Intravascular OCT manufacturers, for example, permit users to specify which contrast agent is used during flushing and link this designation to previously measured index data.

A recent review has identified nearly 100 ophthalmic data repositories containing over half a million OCT images.[202] The situation in other clinical fields is entirely different, possibly owing to the shorter history of commercially available systems; no publicly available repositories appear to be available for cardiovascular, gastrointestinal, or pulmonary OCT. The Mass General Optical Coherence Tomography Registry reports findings based on over 3000 international intravascular OCT cases.[203] Another private database, The International Pediatric OCT Registry, investigates the use of OCT for early detection of coronary vascular changes in children and adolescents after cardiac transplantation.[204]

Limitations and optimisations

Image quality

Perhaps the most confounding characteristic of OCT that inhibits the consistent interpretation of medical images is the phenomenon of speckle: a mottled-appearing artifact of bright and dark features, on a scale near that of the resolution, that arises from coherent interference of the light scattered from the sample. Speckle is inherent to all spatially coherent imaging modalities, including ultrasonography and confocal microscopy. The significance of speckle is evident by the large body of research dedicated to its mitigation; a search using Google Scholar and keywords speckle, reduction, and OCT, yields over 30,000 results. Strategies to reduce speckle essentially rely on the incoherent averaging of multiple images wherein the sample structure is consistent while the speckle realization is uncorrelated. While some of the methods that have been reported have shown benefit with some impairment of resolution, there remains an important opportunity for new approaches in this area.

A second significant general limitation of OCT is its depth of penetration. In most biological tissues, the penetration depth is limited by scattering to a few mm. While scattering falls monotonically with increasing wavelength, the scaling is not strong and moving to wavelengths longer than 1300 nm is complicated by the paucity of high quality optical and fiber optical devices and components. Fortunately, internal organs can be accessed by narrow diameter, flexible catheters and endoscopes that may be inserted through luminal channels or minimally invasive incisions. Imaging catheters as small as 300 μm have been demonstrated, which are compatible with needle access.[205]

For any imaging modality, the contrast between different tissue or cellular elements is essential. Endogenous contrast in OCT arises from variations in the backscattering cross-section of various tissue components. Fortunately, the dynamic range of OCT is typically on the order of 50 dB and many tissue exhibit significant structure in OCT images. Additionally, spectroscopic OCT has been applied to enhance endogenous contrast through analysis of spectrally-dependent reflectance.[206] Further, several approaches have been developed to introduce labeled, exogenous contrast agents in OCT.[207–209]

Author Manuscript Author Manuscript Author Manuscript Author Manuscript

While OCT has become the gold standard for the diagnosis and monitoring of retinal pathology and OCT angiography is an attractive modality for observing vascular disorders, it has not fully replaced the need for fluorescein angiography. Since OCT angiography relies on blood flow for contrast, it cannot be used to detect leaky vessels. Additionally, there remains a need for wider field of view imaging and for achieving high resolution OCT without dilating the pupil.

Blood is highly attenuating in OCT and intravascular imaging presently relies on the infusion of saline or contrast agents to temporarily displace blood. This adds complications to the procedure and in some patients is contraindicated by renal insufficiency. As imaging speeds continue to increase, the required injection volume will decrease and benign agents such as dextran are potential solutions. An important role for intravascular imaging is in measuring the reference vessel diameter to determine the optimal stent size. This entails measurement of the cross-sectional area of the media at locations distal and proximal to the stenosis that will be treated. The contrast of the media on reflectance OCT may not always be sufficient for robust automated measurement algorithms. Fortunately, PS-OCT appears to provide a much more consistent contrast of the media based on birefringence and this may prove to be a more robust basis for automated measurements. Another significant limitation for intravascular OCT is in the depth of penetration of lipid rich plaques where scattering can be very high. The development of hybrid ultrasound and OCT catheters appears to be a solution to this dilemma, and a commercial hybrid product is available.[210,211]

In gastrointestinal endoscopy and pulmonary bronchoscopy, image criteria have been identified and validated for detecting early neoplastic changes. While the application of these criteria by expert readers has underpinned most research studies, the broad dissemination of OCT will undoubtedly require automated procedures. With the rise of powerful artificial intelligence algorithms for machine learning and machine vision and the availability of the required large training datasets, it is likely that automated diagnosis will become routine. At present, the cost of endoscopic and bronchoscopic procedures through which OCT is delivered is high and the application to screening roles is not economically practical. The advent of strategies like tethered capsule endoscopy that circumvent the need for conscious sedation and the cost of endoscopy may overcome this limitation.

Outlook

The availability of high performance, compact, and inexpensive optical components is essential for the widespread dissemination of OCT instrumentation. Early development in the field depended upon the synergistic interests of the telecommunications industry for the photonic components required for OCT light sources, interferometers, and detectors. As OCT commercialization expanded and diversified, component performance has continued to increase as prices have dropped. The materials cost for OCT consoles remains influential when contemplating new clinical strategies and opportunities, however, and further advances will be necessary to sustain growth in the field. The size of OCT instrumentation is also important, as it would be advantageous to better integrate hardware seamlessly into specific clinical environments.

Author Manuscript Author Manuscript Author Manuscript Author Manuscript

Advances in computing resources and artificial intelligence will undoubtedly be major factors in the future of the OCT field. Graphical processing units, which have largely been developed for computer gaming, offer major opportunities for accelerated numerical processing with compact, low power, and economical hardware. The promise of machine learning for automated image interpretation and quantification is widely appreciated in medical imaging and as OCT data becomes more readily available, advances in these areas for OCT will play increasingly important roles. While the primary focus in these areas will be on advanced diagnostic roles and in guiding intervention, there are also opportunities for artificial intelligence in signal processing roles, such as speckle mitigation and functional imaging.

While computational speed is one factor for OCT performance, fast image acquisition also requires advances in light sources for frequency domain and digital cameras for spectral domain. Currently, the fastest fd-OCT lasers that have been integrated into commercial medical imaging systems enable A-line acquisition rates of 100 kHz. Increasing this speed by 10- or even 100-fold may be possible as prototypes of novel laser designs become refined. It is less clear what might be possible with advances in high speed digital cameras, but rates approaching 1 MHz may be possible. In both cases, these improvements will be clinically significant for wider field of view imaging with fewer motion artifacts and fewer constraints on clinical procedures.

OCT has already enriched the clinical understanding of many ocular diseases and it has been increasingly relied upon for intraoperative guidance. Improvements in large volume, three dimensional imaging will be important for advancing these roles in refractive surgery and the treatment of cataracts and glaucoma. New strategies for wide field angiography and quantitative flow measurements may also be important for the diagnosis of retinal diseases. The prospects for using OCT and functional imaging for detecting retinal changes in advance of cognitive deficits in Alzheimer’s disease has drawn significant interest and could play a prominent role in the future of the field.

Prospective, multi center cardiovascular studies seek to quantify potential improvements in the outcome of coronary treatments guided by imaging compared with conventional intervention. The outcome of these studies will be pivotal for the field as they could identify a role for intravascular OCT in the standard of care treatment of coronary lesions meeting the current criteria for percutaneous intervention. With roughly 4 million procedures currently being performed annually, such a role would significantly increase intravascular OCT use. Further, there is a potential role for coronary OCT to comprehensively screen main coronary arteries in patients undergoing intervention for disease that may give rise to future events. This capability would not only increase OCT use but would also enable new therapeutic procedures to prevent heart attack.

In gastrointestinal imaging, current OCT procedures are performed adjunct to white light endoscopy through the use of imaging catheters that are inserted through the endoscope instrument channel. Although this approach has been compatible with research and early dissemination strategies, faster and more streamlined operation is desirable. Integration of OCT functionality directly into the endoscope and increased imaging speed could enable a

Author Manuscript Author Manuscript Author Manuscript Author Manuscript

reduction of procedure time from what is currently several minutes to seconds. The advent of tethered capsule OCT also opens the fundamentally new opportunity for diagnostic esophageal screening, as comprehensive upper GI imaging is now possible in unsedated patients, thereby drastically reducing cost and overall procedure time.

The navigation of OCT imaging catheters is uniquely important for pulmonary imaging. While early clinical studies have required bronchoscope actuation for directing an OCT catheter, tailored designs will be required to navigate the complex pulmonary anatomy. In addition to mechanically actuated catheters, interstitial OCT probes, perhaps mimicking biopsy needles, will be required to reach regions of lung beyond the boundaries of the airway wall.

Across all clinical fields, future integration of OCT hardware into the specific clinical environments will be important. Aside from guided corneal refractive surgery instruments, OCT is currently deployed as a stand-alone system or console. Reductions in system size and cost would enable advanced OCT capabilities to be seamlessly deployed within standard clinical infrastructure. Coupled with the overall trend of accelerating progress in OCT technology development and the breadth of OCT research programs internationally, integration and dissemination will drive future clinical growth and adoption.

Competing interests

BEB, JFdB, BV, and MV are inventors on patents owned by Mass General Brigham in the field of OCT and acknowledge patent royalties, administered through MassGeneral Brigham, from organizations that may gain or lose financially through this publication.

IKJ has received educational grants from Abbott Vascular and consulting fees from Svelte Medical Systems, Inc. and Mitobridge, Inc.

DH and Oregon Health & Science University (OHSU) have significant financial interests in an organization that may gain or lose financially through this publication. DH acknowledges research support and patent royalty from an organization that may gain or lose financially through this publication.

DDS is an inventor on patents owned by the University of Western Australia in the field of OCT and licensed to organizations that may gain or lose financially through this publication.

Bibliography

1. Huang D et al. Optical coherence tomography. science 254, 1178–1181 (1991). [PubMed: 1957169]
2. Youngquist RC, Carr S & Davies DE Optical coherence-domain reflectometry: a new optical evaluation technique. Optics letters 12, 158–160 (1987). [PubMed: 19738824]
3. Eickhoff W & Ulrich R Optical frequency domain reflectometry in single-mode fiber. Applied Physics Letters 39, 693–695 (1981).
4. Fercher A, Mengedoht K & Werner W Eye-length measurement by interferometry with partially coherent light. Optics letters 13, 186–188 (1988). [PubMed: 19742022]
5. Hee MR, Huang D, Swanson EA & Fujimoto JG Polarization-sensitive low-coherence reflectometer for birefringence characterization and ranging. J. Opt. Soc. Am. B 9, 903–908, doi:10.1364/JOSAB.9.000903 (1992).
6. de Boer JF in Frontiers in Optics. FWA6 (Optical Society of America).
7. Wang X, Milner T & Nelson J Characterization of fluid flow velocity by optical Doppler tomography. Optics letters 20, 1337–1339 (1995). [PubMed: 19859518]

Author Manuscript Author Manuscript Author Manuscript Author Manuscript

8. Schmitt JM OCT elastography: imaging microscopic deformation and strain of tissue. Optics express 3, 199–211 (1998). [PubMed: 19384362]
9. Bouma B et al. High-resolution optical coherence tomographic imaging using a mode-locked Ti:Al_2O_3laser source. Optics Letters 20, 1486–1488 (1995). [PubMed: 19862057]
10. Bouma BE, Tearney GJ, Bilinsky IP, Golubovic B & Fujimoto JG Self-phase-modulated Kerr-lens mode-locked Cr:forsterite laser source for optical coherence tomography. Optics Letters 21, 1839–1841 (1996). [PubMed: 19881819]
11. Tearney G, Bouma B & Fujimoto J High-speed phase-and group-delay scanning with a grating-based phase control delay line. Optics letters 22, 1811–1813 (1997). [PubMed: 18188374]
12. Tearney G et al. Scanning single-mode fiber optic catheter–endoscope for optical coherence tomography. Optics letters 21, 543–545 (1996). [PubMed: 19865466]
13. Tearney GJ et al. In vivo endoscopic optical biopsy with optical coherence tomography. Science 276, 2037–2039 (1997). [PubMed: 9197265]
14. Choma MA, Sarunic MV, Yang C & Izatt JA Sensitivity advantage of swept source and Fourier domain optical coherence tomography. Optics express 11, 2183–2189 (2003). [PubMed: 19466106]
15. Leitgeb R, Hitzenberger C & Fercher AF Performance of fourier domain vs. time domain optical coherence tomography. Optics express 11, 889–894 (2003). [PubMed: 19461802]
16. de Boer JF et al. Improved signal-to-noise ratio in spectral-domain compared with time-domain optical coherence tomography. Optics Letters 28, 2067–2069 (2003). [PubMed: 14587817]
17. Yun SH, Tearney GJ, de Boer JF, Iftimia N & Bouma BE High-speed optical frequency-domain imaging. Optics Express 11, 2953–2963 (2003). [PubMed: 19471415]
18. Cense B et al. Ultrahigh-resolution high-speed retinal imaging using spectral-domain optical coherence tomography. Optics express 12, 2435–2447 (2004). [PubMed: 19475080]
19. Wojtkowski M et al. Ultrahigh-resolution, high-speed, Fourier domain optical coherence tomography and methods for dispersion compensation. Optics express 12, 2404–2422 (2004). [PubMed: 19475077]
20. Swanson E & Huang D Ophthalmic OCT reaches $1 billion per year. Retinal Physician 8, 45 (2011).
21. Fahed AC & Jang I-K Plaque erosion and acute coronary syndromes: phenotype, molecular characteristics and future directions. Nature Reviews Cardiology 18, 724–734, doi:10.1038/s41569-021-00542-3 (2021). [PubMed: 33953381]
22. Leggett CL et al. Comparative diagnostic performance of volumetric laser endomicroscopy and confocal laser endomicroscopy in the detection of dysplasia associated with Barrett's esophagus. Gastrointest Endosc 83, 880–888.e882, doi:10.1016/j.gie.2015.08.050 (2016). [PubMed: 26344884]
23. Hariri LP et al. Volumetric optical frequency domain imaging of pulmonary pathology with precise correlation to histopathology. Chest 143, 64–74 (2013). [PubMed: 22459781]
24. Vakoc BJ et al. Three-dimensional microscopy of the tumor microenvironment in vivo using optical frequency domain imaging. Nature medicine 15, 1219–1223 (2009).
25. Izatt JA, Hee MR, Owen GM, Swanson EA & Fujimoto JG Optical coherence microscopy in scattering media. Optics letters 19, 590–592 (1994). [PubMed: 19844382]
26. Beaurepaire E, Boccara AC, Lebec M, Blanchot L & Saint-Jalmes H Full-field optical coherence microscopy. Optics letters 23, 244–246 (1998). [PubMed: 18084473]
27. Vinegoni C et al. in Coherence Domain Optical Methods and Optical Coherence Tomography in Biomedicine X. 226–233 (SPIE).
28. Ughi GJ et al. Clinical characterization of coronary atherosclerosis with dual-modality OCT and near-infrared autofluorescence imaging. JACC: Cardiovascular imaging 9, 1304–1314 (2016). [PubMed: 26971006]
29. Bouma BE & Tearney GJ Power-efficient nonreciprocal interferometer and linear-scanning fiber-optic catheter for optical coherence tomography. Optics Letters 24, 531–533 (1999). [PubMed: 18071562]

Author Manuscript Author Manuscript Author Manuscript Author Manuscript

30. Rollins AM & Izatt JA Optimal interferometer designs for optical coherence tomography. Optics letters 24, 1484–1486 (1999). [PubMed: 18079840]
31. Wojtkowski M, Kowalczyk A, Leitgeb R & Fercher A Full range complex spectral optical coherence tomography technique in eye imaging. Optics letters 27, 1415–1417 (2002). [PubMed: 18026464]
32. Nassif N et al. In vivo human retinal imaging by ultrahigh-speed spectral domain optical coherence tomography. Optics letters 29, 480–482 (2004). [PubMed: 15005199]
33. Yun S, Tearney G, De Boer J & Bouma B Pulsed-source and swept-source spectral-domain optical coherence tomography with reduced motion artifacts. Optics Express 12, 5614–5624 (2004). [PubMed: 19488195]
34. Häusler G & Lindner MW “Coherence radar” and” spectral radar”-new tools for dermatological diagnosis. Journal of biomedical optics 3, 21–31 (1998). [PubMed: 23015002]
35. Yun S, Tearney G, Bouma B, Park B & de Boer JF High-speed spectral-domain optical coherence tomography at 1.3 μm wavelength. Optics express 11, 3598–3604 (2003). [PubMed: 19471496]
36. Tozburun S, Blatter C, Siddiqui M, Meijer EF & Vakoc BJ Phase-stable Doppler OCT at 19 MHz using a stretched-pulse mode-locked laser. Biomedical optics express 9, 952–961 (2018). [PubMed: 29541496]
37. Huber R, Wojtkowski M, Fujimoto JG, Jiang J & Cable A Three-dimensional and C-mode OCT imaging with a compact, frequency swept laser source at 1300 nm. Optics express 13, 10523–10538 (2005). [PubMed: 19503267]
38. Wieser W, Biedermann BR, Klein T, Eigenwillig CM & Huber R Multi-megahertz OCT: High quality 3D imaging at 20 million A-scans and 4.5 GVoxels per second. Optics express 18, 14685–14704, doi:10.1364/OE.18.014685 (2010). [PubMed: 20639955]
39. Xu J et al. High-performance multi-megahertz optical coherence tomography based on amplified optical time-stretch. Biomedical optics express 6, 1340–1350, doi:10.1364/BOE.6.001340 (2015). [PubMed: 25909017]
40. Wang Z et al. Cubic meter volume optical coherence tomography. Optica 3, 1496–1503, doi:10.1364/OPTICA.3.001496 (2016). [PubMed: 28239628]
41. Siddiqui M & Vakoc BJ Optical-domain subsampling for data efficient depth ranging in Fourier-domain optical coherence tomography. Optics Express 20, 17938, doi:10.1364/OE.20.017938 (2012). [PubMed: 23038343]
42. Kolb JP et al. Live video rate volumetric OCT imaging of the retina with multi-MHz A-scan rates. PloS one 14, e0213144, doi:10.1371/journal.pone.0213144 (2019). [PubMed: 30921342]
43. Lippok N, Siddiqui M, Vakoc BJ & Bouma BE Extended Coherence Length and Depth Ranging Using a Fourier-Domain Mode-Locked Frequency Comb and Circular Interferometric Ranging. Physical Review Applied 11, 014018, doi:10.1103/PhysRevApplied.11.014018, eprint = 1810.07769 (2019).
44. Lippok N, Bouma BE & Vakoc BJ Stable multi-megahertz circular-ranging optical coherence tomography at 1.3 μm. Biomedical Optics Express 11, 174, doi:10.1364/BOE.11.000174 (2020). [PubMed: 32010508]
45. Tsai T-H, Zhou C, Adler DC & Fujimoto JG Frequency comb swept lasers. Optics express 17, 21257–21270, doi:10.1364/OE.17.021257 (2009). [PubMed: 19997365]
46. Diddams SA, Vahala K & Udem T Optical frequency combs: Coherently uniting the electromagnetic spectrum. Science (New York, N.Y.) 369, doi:10.1126/science.aay3676 (2020).
47. Khazaeinezhad R, Siddiqui M & Vakoc BJ 16 MHz wavelength-swept and wavelength-stepped laser architectures based on stretched-pulse active mode locking with a single continuously chirped fiber Bragg grating. Optics Letters 42, 2046, doi:10.1364/OL.42.002046 (2017). [PubMed: 28504745]
48. Siddiqui M et al. High-speed optical coherence tomography by circular interferometric ranging. Nature Photonics 12, 111–116, doi:10.1038/s41566-017-0088-x (2018). [PubMed: 29657576]
49. Lippok N & Vakoc BJ Resolving absolute depth in circular-ranging optical coherence tomography by using a degenerate frequency comb. Optics Letters 45, 1079, doi:10.1364/OL.389085 (2020). [PubMed: 32108774]

Author Manuscript Author Manuscript Author Manuscript Author Manuscript

50. Kim TS & Vakoc BJ Stepped frequency comb generation based on electro-optic phase-code mode-locking for moderate-speed circular-ranging OCT. Biomedical Optics Express 11, 3534, doi:10.1364/BOE.392359 (2020). [PubMed: 33014549]
51. Baumann B Polarization sensitive optical coherence tomography: a review of technology and applications. Applied Sciences 7, 474 (2017).
52. De Boer JF, Hitzenberger CK & Yasuno Y Polarization sensitive optical coherence tomography–a review. Biomedical optics express 8, 1838–1873 (2017). [PubMed: 28663869]
53. Park BH et al. Real-time fiber-based multi-functional spectral-domain optical coherence tomography at 1.3 μm. Optics express 13, 3931–3944 (2005). [PubMed: 19495302]
54. Oh W-Y et al. High-speed polarization sensitive optical frequency domain imaging with frequency multiplexing. Optics express 16, 1096–1103 (2008). [PubMed: 18542183]
55. Makita S, Yamanari M & Yasuno Y Generalized Jones matrix optical coherence tomography: performance and local birefringence imaging. Optics express 18, 854–876 (2010). [PubMed: 20173907]
56. Saxer CE et al. High-speed fiber–based polarization-sensitive optical coherence tomography of in vivo human skin. Optics letters 25, 1355–1357 (2000). [PubMed: 18066215]
57. Baumann B et al. Swept source/Fourier domain polarization sensitive optical coherence tomography with a passive polarization delay unit. Optics express 20, 10229–10241 (2012). [PubMed: 22535114]
58. Lim Y, Hong Y, Duan L & Yasuno Y in Biomedical Optics. BTu2B. 4 (Optical Society of America).
59. Villiger M et al. Optic axis mapping with catheter-based polarization-sensitive optical coherence tomography. Optica 5, 1329–1337 (2018). [PubMed: 31214632]
60. Hitzenberger CK, Götzinger E, Sticker M, Pircher M & Fercher AF Measurement and imaging of birefringence and optic axis orientation by phase resolved polarization sensitive optical coherence tomography. Optics express 9, 780–790 (2001). [PubMed: 19424315]
61. Trasischker W et al. Single input state polarization sensitive swept source optical coherence tomography based on an all single mode fiber interferometer. Biomedical optics express 5, 2798–2809 (2014). [PubMed: 25136503]
62. Götzinger E, Baumann B, Pircher M & Hitzenberger CK Polarization maintaining fiber based ultra-high resolution spectral domain polarization sensitive optical coherence tomography. Optics express 17, 22704–22717 (2009). [PubMed: 20052196]
63. Al-Qaisi MK & Akkin T Swept-source polarization-sensitive optical coherence tomography based on polarization-maintaining fiber. Opt Express 18, 3392–3403, doi:10.1364/oe.18.003392 (2010). [PubMed: 20389349]
64. Xiong Q et al. Constrained polarization evolution simplifies depth-resolved retardation measurements with polarization-sensitive optical coherence tomography. Biomedical Optics Express 10, 5207–5222 (2019). [PubMed: 31646042]
65. Zhao Y et al. Phase-resolved optical coherence tomography and optical Doppler tomography for imaging blood flow in human skin with fast scanning speed and high velocity sensitivity. Optics letters 25, 114–116 (2000). [PubMed: 18059800]
66. Leitgeb RA, Werkmeister RM, Blatter C & Schmetterer L Doppler optical coherence tomography. Progress in retinal and eye research 41, 26–43 (2014). [PubMed: 24704352]
67. Makita S, Hong Y, Yamanari M, Yatagai T & Yasuno Y Optical coherence angiography. Optics express 14, 7821–7840 (2006). [PubMed: 19529151]
68. Spaide RF, Fujimoto JG, Waheed NK, Sadda SR & Staurenghi G Optical coherence tomography angiography. Progress in retinal and eye research 64, 1–55 (2018). [PubMed: 29229445]
69. Blatter C et al. Ultrahigh-speed non-invasive widefield angiography. Journal of biomedical optics 17, 070505 (2012). [PubMed: 22894461]
70. Salas M et al. Compact akinetic swept source optical coherence tomography angiography at 1060 nm supporting a wide field of view and adaptive optics imaging modes of the posterior eye. Biomedical Optics Express 9, 1871–1892 (2018). [PubMed: 29675326]
71. Grulkowski I et al. Scanning protocols dedicated to smart velocity ranging in spectral OCT. Optics Express 17, 23736–23754 (2009). [PubMed: 20052085]

Author Manuscript Author Manuscript Author Manuscript Author Manuscript

72. Ploner SB et al. Toward quantitative optical coherence tomography angiography: visualizing blood flow speeds in ocular pathology using variable interscan time analysis. Retina 36, S118–S126 (2016). [PubMed: 28005670]
73. Poddar R & Werner JS Implementations of three OCT angiography (OCTA) methods with 1.7 MHz A-scan rate OCT system on imaging of human retinal and choroidal vasculature. Optics & Laser Technology 102, 130–139 (2018).
74. Barton JK & Stromski S Flow measurement without phase information in optical coherence tomography images. Optics express 13, 5234–5239 (2005). [PubMed: 19498514]
75. Liu GY et al. High power wavelength linearly swept mode locked fiber laser for OCT imaging. Optics express 16, 14095–14105 (2008). [PubMed: 18773019]
76. Zhao Y et al. Doppler standard deviation imaging for clinical monitoring of in vivo human skin blood flow. Optics letters 25, 1358–1360 (2000). [PubMed: 18066216]
77. Kim DY et al. In vivo volumetric imaging of human retinal circulation with phase-variance optical coherence tomography. Biomedical optics express 2, 1504–1513 (2011). [PubMed: 21698014]
78. An L, Qin J & Wang RK Ultrahigh sensitive optical microangiography for in vivo imaging of microcirculations within human skin tissue beds. Optics express 18, 8220–8228 (2010). [PubMed: 20588668]
79. Gorczynska I, Migacz JV, Zawadzki RJ, Capps AG & Werner JS Comparison of amplitude-decorrelation, speckle-variance and phase-variance OCT angiography methods for imaging the human retina and choroid. Biomedical optics express 7, 911–942 (2016). [PubMed: 27231598]
80. Gräfe MG, Nadiarnykh O & De Boer JF Optical coherence tomography velocimetry based on decorrelation estimation of phasor pair ratios (DEPPAIR). Biomedical Optics Express 10, 5470–5485 (2019). [PubMed: 31799025]
81. Alam SK & Garra BS Tissue elasticity imaging: volume 1: theory and methods. (Elsevier, 2019).
82. Kennedy BF, Wijesinghe P & Sampson DD The emergence of optical elastography in biomedicine. Nature Photonics 11, 215–221 (2017).
83. Larin KV & Sampson DD Optical coherence elastography–OCT at work in tissue biomechanics. Biomedical optics express 8, 1172–1202 (2017). [PubMed: 28271011]
84. Kennedy BF (AIP Publishing LLC, 2021).
85. Liu C-H et al. Nanobomb optical coherence elastography. Optics letters 43, 2006–2009 (2018). [PubMed: 29714732]
86. Zvietcovich F, Pongchalee P, Meemon P, Rolland JP & Parker KJ Reverberant 3D optical coherence elastography maps the elasticity of individual corneal layers. Nature communications 10, 1–13 (2019).
87. Kennedy BF et al. Optical coherence micro-elastography: mechanical-contrast imaging of tissue microstructure. Biomedical optics express 5, 2113–2124 (2014). [PubMed: 25071952]
88. Kennedy KM et al. Quantitative micro-elastography: imaging of tissue elasticity using compression optical coherence elastography. Scientific reports 5, 1–12 (2015).
89. Dong L et al. Volumetric quantitative optical coherence elastography with an iterative inversion method. Biomedical Optics Express 10, 384–398 (2019). [PubMed: 30800487]
90. Pelivanov I et al. Does group velocity always reflect elastic modulus in shear wave elastography? Journal of biomedical optics 24, 076003 (2019). [PubMed: 31342691]
91. Podoleanu AG Optical coherence tomography. The British journal of radiology 78, 976–988 (2005). [PubMed: 16249597]
92. Zawadzki RJ et al. Adaptive-optics optical coherence tomography for high-resolution and high-speed 3D retinal in vivo imaging. Optics express 13, 8532–8546 (2005). [PubMed: 19096728]
93. Grulkowski I et al. Anterior segment imaging with Spectral OCT system using a high-speed CMOS camera. Optics express 17, 4842–4858 (2009). [PubMed: 19293916]
94. Schuman JS et al. Quantification of nerve fiber layer thickness in normal and glaucomatous eyes using optical coherence tomography: a pilot study. Archives of ophthalmology 113, 586–596 (1995). [PubMed: 7748128]

Author Manuscript Author Manuscript Author Manuscript Author Manuscript

95. Wang Y, Bower BA, Izatt JA, Tan O & Huang D Retinal blood flow measurement by circumpapillary Fourier domain Doppler optical coherence tomography. Journal of biomedical optics 13, 064003 (2008). [PubMed: 19123650]
96. Srinivasan VJ et al. High-definition and 3-dimensional imaging of macular pathologies with high-speed ultrahigh-resolution optical coherence tomography. Ophthalmology 113, 2054–2065 (2006).
97. Wojtkowski M et al. Three-dimensional retinal imaging with high-speed ultrahigh-resolution optical coherence tomography. Ophthalmology 112, 1734–1746 (2005). [PubMed: 16140383]
98. Hee MR et al. Quantitative assessment of macular edema with optical coherence tomography. Arch Ophthalmol 113, 1019–1029 (1995). [PubMed: 7639652]
99. Hee MR et al. Optical coherence tomography of the human retina. Arch Ophthalmol 113, 325–332 (1995). [PubMed: 7887846]
100. Hee MR Artifacts in optical coherence tomography topographic maps. Am J Ophthalmol 139, 154–155 (2005). [PubMed: 15652841]
101. Szkulmowski M et al. Analysis of posterior retinal layers in spectral optical coherence tomography images of the normal retina and retinal pathologies. Journal of Biomedical Optics 12, - (2007).
102. Karnowski K, Kaluzny BJ, Szkulmowski M, Gora M & Wojtkowski M Corneal topography with high-speed Swept Source OCT in clinical examination. Biomedical Optics Express 9, 2709–2720 (2011).
103. Gora M et al. Ultra high-speed swept source OCT imaging of the anterior segment of human eye at 200 kHz with adjustable imaging range. Opt Express 17, 14880–14894, doi:184430 [pii] (2009). [PubMed: 19687967]
104. Yun SH et al. Comprehensive volumetric optical microscopy in vivo. Nature Medicine 12, 1429–1433 (2006).
105. Athanasiou LS et al. Methodology for fully automated segmentation and plaque characterization in intracoronary optical coherence tomography images. Journal of biomedical optics 19, 026009 (2014). [PubMed: 24525828]
106. Ughi GJ et al. Automated segmentation and characterization of esophageal wall in vivo by tethered capsule optical coherence tomography endomicroscopy. Biomedical optics express 7, 409–419 (2016). [PubMed: 26977350]
107. Park BH, Pierce MC, Cense B & De Boer JF Optic axis determination accuracy for fiber-based polarization-sensitive optical coherence tomography. Optics letters 30, 2587–2589 (2005). [PubMed: 16208908]
108. Todorović M, Jiao S, Wang LV & Stoica G Determination of local polarization properties of biological samples in the presence of diattenuation by use of Mueller optical coherence tomography. Optics letters 29, 2402–2404 (2004). [PubMed: 15532281]
109. Lu S-Y & Chipman RA Homogeneous and inhomogeneous Jones matrices. JOSA A 11, 766–773 (1994).
110. Park BH, Pierce MC, Cense B & De Boer JF Real-time multi-functional optical coherence tomography. Optics express 11, 782–793 (2003). [PubMed: 19461791]
111. Villiger M et al. Spectral binning for mitigation of polarization mode dispersion artifacts in catheter-based optical frequency domain imaging. Optics express 21, 16353–16369 (2013). [PubMed: 23938487]
112. Villiger M et al. Deep tissue volume imaging of birefringence through fibre-optic needle probes for the delineation of breast tumour. Scientific reports 6, 1–11 (2016). [PubMed: 28442746]
113. Fan C & Yao G Imaging myocardial fiber orientation using polarization sensitive optical coherence tomography. Biomedical optics express 4, 460–465 (2013). [PubMed: 23504508]
114. Zhang EZ & Vakoc BJ Polarimetry noise in fiber-based optical coherence tomography instrumentation. Optics express 19, 16830–16842 (2011). [PubMed: 21935044]
115. Villiger M et al. Artifacts in polarization-sensitive optical coherence tomography caused by polarization mode dispersion. Optics letters 38, 923–925 (2013). [PubMed: 23503261]

Author Manuscript Author Manuscript Author Manuscript Author Manuscript

116. Braaf B, Vermeer KA, de Groot M, Vienola KV & de Boer JF Fiber-based polarization-sensitive OCT of the human retina with correction of system polarization distortions. Biomedical optics express 5, 2736–2758 (2014). [PubMed: 25136498]
117. Aiello A & Woerdman JP Role of spatial coherence in polarization tomography. Opt Lett 30, 1599–1601, doi:10.1364/ol.30.001599 (2005). [PubMed: 16075509]
118. Adie SG, Hillman TR & Sampson DD Detection of multiple scattering in optical coherence tomography using the spatial distribution of Stokes vectors. Opt Express 15, 18033–18049, doi:10.1364/oe.15.018033 (2007). [PubMed: 19551101]
119. Götzinger E et al. Retinal pigment epithelium segmentation by polarization sensitive optical coherence tomography. Optics express 16, 16410–16422 (2008). [PubMed: 18852747]
120. Villiger M et al. Coronary plaque microstructure and composition modify optical polarization: a new endogenous contrast mechanism for optical frequency domain imaging. JACC: Cardiovascular Imaging 11, 1666–1676 (2018). [PubMed: 29248662]
121. Lippok N et al. Depolarization signatures map gold nanorods within biological tissue. Nature photonics 11, 583–588 (2017). [PubMed: 29201136]
122. Takusagawa HL et al. Projection-resolved optical coherence tomography angiography of macular retinal circulation in glaucoma. Ophthalmology 124, 1589–1599 (2017). [PubMed: 28676279]
123. Laíns I et al. Retinal applications of swept source optical coherence tomography (OCT) and optical coherence tomography angiography (OCTA). Progress in retinal and eye research 84, 100951 (2021). [PubMed: 33516833]
124. Tsai T-H et al. Endoscopic optical coherence angiography enables 3-dimensional visualization of subsurface microvasculature. Gastroenterology 147, 1219–1221 (2014). [PubMed: 25172015]
125. Wurster LM et al. Comparison of optical coherence tomography angiography and narrow-band imaging using a bimodal endoscope. Journal of Biomedical Optics 25, 032003 (2019). [PubMed: 31562707]
126. Schmoll T et al. Imaging of the parafoveal capillary network and its integrity analysis using fractal dimension. Biomedical optics express 2, 1159–1168 (2011). [PubMed: 21559128]
127. Meiburger KM et al. Automatic skin lesion area determination of basal cell carcinoma using optical coherence tomography angiography and a skeletonization approach: Preliminary results. Journal of biophotonics 12, e201900131 (2019). [PubMed: 31100191]
128. Yao X, Alam MN, Le D & Toslak D Quantitative optical coherence tomography angiography: a review. Experimental Biology and Medicine 245, 301–312 (2020). [PubMed: 31958986]
129. Gao M et al. Reconstruction of high-resolution 6× 6-mm OCT angiograms using deep learning. Biomedical Optics Express 11, 3585–3600 (2020). [PubMed: 33014553]
130. Tsokolas G, Tsaousis KT, Diakonis VF, Matsou A & Tyradellis S Optical coherence tomography angiography in neurodegenerative diseases: a review. Eye and *brain* 12, 73 (2020).
131. Pitre JJ et al. Nearly-incompressible transverse isotropy (NITI) of cornea elasticity: model and experiments with acoustic micro-tapping OCE. Scientific reports 10, 1–14 (2020). [PubMed: 31913322]
132. De Stefano VS, Ford MR, Seven I & Dupps WJ Depth-dependent corneal biomechanical properties in normal and keratoconic subjects by optical coherence elastography. Translational Vision Science & Technology 9, 4–4 (2020).
133. Kennedy KM et al. Diagnostic accuracy of quantitative micro-elastography for margin assessment in breast-conserving surgery. Cancer research 80, 1773–1783 (2020). [PubMed: 32295783]
134. Hadden WJ et al. Stem cell migration and mechanotransduction on linear stiffness gradient hydrogels. Proceedings of the National Academy of Sciences 114, 5647–5652 (2017).
135. Wijesinghe P et al. Ultrahigh-resolution optical coherence elastography images cellular-scale stiffness of mouse aorta. Biophysical journal 113, 2540–2551 (2017). [PubMed: 29212007]
136. Mulligan JA, Ling L, Leartprapun N, Fischbach C & Adie SG Computational 4D-OCM for label-free imaging of collective cell invasion and force-mediated deformations in collagen. Scientific reports 11, 1–13 (2021). [PubMed: 33414495]
137. Swanson EA et al. In vivo retinal imaging by optical coherence tomography. Optics letters 18, 1864–1866 (1993). [PubMed: 19829430]

Author Manuscript Author Manuscript Author Manuscript Author Manuscript

138. Windsor MA et al. Estimating public and patient savings from basic research—a study of optical coherence tomography in managing antiangiogenic therapy. American journal of ophthalmology 185, 115–122 (2018). [PubMed: 29224686]
139. Ko TH et al. Comparison of ultrahigh-and standard-resolution optical coherence tomography for imaging macular hole pathology and repair. Ophthalmology 111, 2033–2043 (2004). [PubMed: 15522369]
140. Zhang M et al. Automated quantification of nonperfusion in three retinal plexuses using projection-resolved optical coherence tomography angiography in diabetic retinopathy. Investigative ophthalmology & visual science 57, 5101–5106 (2016). [PubMed: 27699408]
141. Malihi M et al. Optical coherence tomographic angiography of choroidal neovascularization ill-defined with fluorescein angiography. British Journal of Ophthalmology 101, 45–50 (2017). [PubMed: 27913440]
142. You QS et al. Detection of clinically unsuspected retinal neovascularization with wide-field optical coherence tomography angiography. Retina (Philadelphia, Pa.) (2020).
143. Tan O et al. Detection of macular ganglion cell loss in glaucoma by Fourier-domain optical coherence tomography. Ophthalmology 116, 2305–2314. e2302 (2009). [PubMed: 19744726]
144. Chen A et al. Measuring glaucomatous focal perfusion loss in the peripapillary retina using OCT angiography. Ophthalmology 127, 484–491 (2020). [PubMed: 31899032]
145. Zhang X et al. Comparison of glaucoma progression detection by optical coherence tomography and visual field. American journal of ophthalmology 184, 63–74 (2017). [PubMed: 28964806]
146. Li Y et al. Guiding flying-spot laser transepithelial phototherapeutic keratectomy with optical coherence tomography. Journal of Cataract & Refractive Surgery 43, 525–536 (2017). [PubMed: 28532939]
147. Yang Y, Pavlatos E, Chamberlain W, Huang D & Li Y Keratoconus detection using OCT corneal and epithelial thickness map parameters and patterns. Journal of Cataract & Refractive Surgery 47, 759–766 (2021). [PubMed: 33181629]
148. Ma P et al. Evaluation of the Diagnostic Performance of Swept-Source Anterior Segment Optical Coherence Tomography in Primary Angle Closure Disease. American Journal of Ophthalmology 233, 68–77 (2022). [PubMed: 34283974]
149. Wang L, Tang M, Huang D, Weikert MP & Koch DD Comparison of newer intraocular lens power calculation methods for eyes after corneal refractive surgery. Ophthalmology 122, 2443–2449 (2015). [PubMed: 26459996]
150. Libby P Current concepts of the pathogenesis of the acute coronary syndromes. Circulation 104, 365–372, doi:10.1161/01.cir.104.3.365 (2001). [PubMed: 11457759]
151. Jang I-K, Tearney GJ & Bouma BE Visualization of Tissue Prolapse Between Coronary Stent Struts by Optical Coherence Tomography: Comparison With Intravascular Ultrasound. Circulation 104, 2754 (2001). [PubMed: 11723031]
152. Yabushita H et al. Characterization of human atherosclerosis by optical coherence tomography. Circulation 106, 1640–1645 (2002). [PubMed: 12270856]
153. Jang I-K et al. In vivo characterization of coronary atherosclerotic plaque by use of optical coherence tomography. Circulation 111, 1551–1555 (2005). [PubMed: 15781733]
154. Bouma B et al. Evaluation of intracoronary stenting by intravascular optical coherence tomography. Heart 89, 317–320 (2003). [PubMed: 12591841]
155. Tearney GJ et al. Quantification of macrophage content in atherosclerotic plaques by optical coherence tomography. Circulation 107, 113–119 (2003). [PubMed: 12515752]
156. Prati F et al. Expert review document part 2: methodology, terminology and clinical applications of optical coherence tomography for the assessment of interventional procedures. Eur Heart J 33, 2513–2520, doi:10.1093/eurheartj/ehs095 (2012). [PubMed: 22653335]
157. Ali ZA et al. Optical coherence tomography compared with intravascular ultrasound and with angiography to guide coronary stent implantation (ILUMIEN III: OPTIMIZE PCI): a randomised controlled trial. Lancet 388, 2618–2628, doi:10.1016/s0140-6736(16)31922-5 (2016). [PubMed: 27806900]

Author Manuscript Author Manuscript Author Manuscript Author Manuscript

158. Kubo T et al. Optical frequency domain imaging vs. intravascular ultrasound in percutaneous coronary intervention (OPINION trial): one-year angiographic and clinical results. Eur Heart J 38, 3139–3147, doi:10.1093/eurheartj/ehx351 (2017). [PubMed: 29121226]

159. Tamis-Holland JE et al. Contemporary Diagnosis and Management of Patients With Myocardial Infarction in the Absence of Obstructive Coronary Artery Disease: A Scientific Statement From the American Heart Association. Circulation 139, e891–e908, doi:10.1161/cir.0000000000000670 (2019). [PubMed: 30913893]

160. Reynolds HR et al. Coronary Optical Coherence Tomography and Cardiac Magnetic Resonance Imaging to Determine Underlying Causes of Myocardial Infarction With Nonobstructive Coronary Arteries in Women. Circulation 143, 624–640, doi:10.1161/circulationaha.120.052008 (2021). [PubMed: 33191769]

161. Jia H et al. Effective anti-thrombotic therapy without stenting: intravascular optical coherence tomography-based management in plaque erosion (the EROSION study). Eur Heart J 38, 792–800, doi:10.1093/eurheartj/ehw381 (2017). [PubMed: 27578806]

162. Bouma BE, Tearney GJ, Compton CC & Nishioka NS High-resolution imaging of the human esophagus and stomach in vivo using optical coherence tomography. Gastrointest Endosc 51, 467–474 (2000). [PubMed: 10744824]

163. Nguyen TH et al. Prevalence and Predictors of Missed Dysplasia on Index Barrett's Esophagus Diagnosing Endoscopy in a Veteran Population. Clin Gastroenterol Hepatol, doi:10.1016/j.cgh.2021.04.008 (2021).

164. Poneros JM et al. Diagnosis of specialized intestinal metaplasia by optical coherence tomography. Gastroenterology 120, 7–12 (2001). [PubMed: 11208708]

165. Evans JA et al. Optical coherence tomography to identify intramucosal carcinoma and high-grade dysplasia in Barrett's esophagus. Clin Gastroenterol Hepatol 4, 38–43, doi:10.1053/s1542-3565(05)00746-9 (2006). [PubMed: 16431303]

166. Evans JA et al. Identifying intestinal metaplasia at the squamocolumnar junction by using optical coherence tomography. Gastrointest Endosc 65, 50–56, doi:10.1016/j.gie.2006.04.027 (2007). [PubMed: 17137858]

167. Blackshear L, Aranda-Michel E, Wolfsen H, Wallace M & Tearney G Volumetric Laser Endomicroscopy (VLE): An OFDI Case Study of Barrett's Esophagus with Dysplasia: 2163. Official journal of the American College of Gastroenterology| ACG 108, S656 (2013).

168. Suter MJ et al. Esophageal-guided biopsy with volumetric laser endomicroscopy and laser cautery marking: a pilot clinical study. Gastrointest Endosc 79, 886–896 (2014). [PubMed: 24462171]

169. Swager AF et al. Feasibility of laser marking in Barrett's esophagus with volumetric laser endomicroscopy: first-in-man pilot study. Gastrointest Endosc 86, 464–472, doi:10.1016/j.gie.2017.01.030 (2017). [PubMed: 28161451]

170. Wolfsen HC et al. Safety and feasibility of volumetric laser endomicroscopy in patients with Barrett's esophagus (with videos). Gastrointest Endosc 82, 631–640, doi:10.1016/j.gie.2015.03.1968 (2015). [PubMed: 25956472]

171. Trindade AJ et al. Volumetric laser endomicroscopy features of dysplasia at the gastric cardia in Barrett's oesophagus: results from an observational cohort study. BMJ Open Gastroenterol 6, e000340, doi:10.1136/bmjgast-2019-000340 (2019).

172. Hatta W et al. Feasibility of optical coherence tomography for the evaluation of Barrett's mucosa buried underneath esophageal squamous epithelium. Dig Endosc 28, 427–433, doi:10.1111/den.12576 (2016). [PubMed: 26583560]

173. Swager AF et al. Detection of buried Barrett's glands after radiofrequency ablation with volumetric laser endomicroscopy. Gastrointest Endosc 83, 80–88, doi:10.1016/j.gie.2015.05.028 (2016). [PubMed: 26124075]

174. Lo WCY et al. Balloon catheter-based radiofrequency ablation monitoring in porcine esophagus using optical coherence tomography. Biomed Opt Express 10, 2067–2089, doi:10.1364/boe.10.002067 (2019). [PubMed: 31086717]

175. Liang K et al. Ultrahigh speed en face OCT capsule for endoscopic imaging. Biomed Opt Express 6, 1146–1163, doi:10.1364/boe.6.001146 (2015). [PubMed: 25909001]

Author Manuscript Author Manuscript Author Manuscript Author Manuscript

176. Gora MJ et al. Tethered capsule endomicroscopy for microscopic imaging of the esophagus, stomach, and duodenum without sedation in humans (with video). Gastrointest Endosc 88, 830–840.e833, doi:10.1016/j.gie.2018.07.009 (2018). [PubMed: 30031805]
177. Pfau PR et al. Criteria for the diagnosis of dysplasia by endoscopic optical coherence tomography. Gastrointest Endosc 58, 196–202, doi:10.1067/mge.2003.344 (2003). [PubMed: 12872085]
178. Shen B et al. In vivo colonoscopic optical coherence tomography for transmural inflammation in inflammatory bowel disease. Clin Gastroenterol Hepatol 2, 1080–1087, doi:10.1016/s1542-3565(04)00621-4 (2004). [PubMed: 15625653]
179. Masci E et al. Pilot study on the correlation of optical coherence tomography with histology in celiac disease and normal subjects. J Gastroenterol Hepatol 22, 2256–2260, doi:10.1111/j.1440-1746.2006.04725.x (2007). [PubMed: 18031391]
180. Singh P, Chak A, Willis JE, Rollins A & Sivak MV Jr. In vivo optical coherence tomography imaging of the pancreatic and biliary ductal system. Gastrointest Endosc 62, 970–974, doi:10.1016/j.gie.2005.06.054 (2005). [PubMed: 16301046]
181. Tyberg A, Xu MM, Gaidhane M & Kahaleh M Second generation optical coherence tomography: Preliminary experience in pancreatic and biliary strictures. Dig Liver Dis 50, 1214–1217, doi:10.1016/j.dld.2018.05.019 (2018). [PubMed: 29937365]
182. Testoni PA et al. Main pancreatic duct, common bile duct and sphincter of Oddi structure visualized by optical coherence tomography: An ex vivo study compared with histology. Dig Liver Dis 38, 409–414, doi:10.1016/j.dld.2006.02.014 (2006). [PubMed: 16584931]
183. Corral JE et al. Volumetric laser endomicroscopy in the biliary and pancreatic ducts: a feasibility study with histological correlation. Endoscopy 50, 1089–1094, doi:10.1055/a-0631-1634 (2018). [PubMed: 29913531]
184. Testoni PA et al. Intraductal optical coherence tomography for investigating main pancreatic duct strictures. Am J Gastroenterol 102, 269–274, doi:10.1111/j.1572-0241.2006.00940.x (2007). [PubMed: 17100970]
185. James AL & Wenzel S Clinical relevance of airway remodelling in airway diseases. European Respiratory Journal 30, 134–155 (2007). [PubMed: 17601971]
186. Chen Y et al. Validation of human small airway measurements using endobronchial optical coherence tomography. Respir Med 109, 1446–1453 (2015). [PubMed: 26427628]
187. d'Hooghe JNS et al. Optical coherence tomography for identification and quantification of human airway wall layers. PloS one 12, e0184145 (2017). [PubMed: 28981500]
188. Su Z-Q et al. Significance of spirometry and impulse oscillometry for detecting small airway disorders assessment with endobronchial optical coherence tomography in COPD. Int J Chron Obstruct Pulmon Dis 13, 3031–3044 (2018). [PubMed: 30319251]
189. Coxon HO et al. Airway Wall Thickness Assessed Using Computed Tomography and Optical Coherence Tomography. Am J Respir Crit Care Med 177, 1201–1206 (2008). [PubMed: 18310475]
190. Adams DC et al. Quantitative assessment of airway remodelling and response to allergen in asthma. Respirology 24, 1073–1080, doi:10.1111/resp.13521 (2019). [PubMed: 30845351]
191. Adams DC et al. Birefringence microscopy platform for assessing airway smooth muscle structure and function in vivo. Sci Transl Med 8, 359ra131, doi:10.1126/scitranslmed.aag1424 (2016).
192. Vaselli M et al. Polarization Sensitive Optical Coherence Tomography for Bronchoscopic Airway Smooth Muscle Detection in Bronchial Thermoplasty-Treated Patients with Asthma. Chest 160, 432–435 (2021). [PubMed: 33785301]
193. McWilliams A, Lam B & Sutedja T Early proximal lung cancer diagnosis and treatment. The European respiratory journal 33, 656–665, doi:10.1183/09031936.00124608 (2009). [PubMed: 19251801]
194. Lam S et al. In vivo optical coherence tomography imaging of preinvasive bronchial lesions. Clin Cancer Res 14, 2006–2011, doi:10.1158/1078-0432.ccr-07-4418 (2008). [PubMed: 18381938]
195. Tsuboi M et al. Optical coherence tomography in the diagnosis of bronchial lesions. Lung cancer (Amsterdam, Netherlands) 49, 387–394, doi:10.1016/j.lungcan.2005.04.007 (2005). [PubMed: 15922488]

Author Manuscript Author Manuscript Author Manuscript Author Manuscript

196. Michel RG, Kinasewitz GT, Fung KM & Keddissi JI Optical coherence tomography as an adjunct to flexible bronchoscopy in the diagnosis of lung cancer: a pilot study. Chest 138, 984–988, doi:10.1378/chest.10-0753 (2010). [PubMed: 20472863]

197. Hariri LP et al. Seeing beyond the bronchoscope to increase the diagnostic yield of bronchoscopic biopsy. Am J Respir Crit Care Med 187, 125–129, doi:10.1164/rccm.201208-1483OE (2013). [PubMed: 23322794]

198. Hariri LP et al. Toward the guidance of transbronchial biopsy: identifying pulmonary nodules with optical coherence tomography. Chest 144, 1261–1268, doi:10.1378/chest.13-0534 (2013). [PubMed: 23828441]

199. Hariri LP et al. Diagnosing lung carcinomas with optical coherence tomography. Ann Am Thorac Soc 12, 193–201, doi:10.1513/AnnalsATS.201408-370OC (2015). [PubMed: 25562183]

200. Hariri LP et al. Endobronchial Optical Coherence Tomography for Low-Risk Microscopic Assessment and Diagnosis of Idiopathic Pulmonary Fibrosis In Vivo. Am J Respir Crit Care Med 197, 949–952, doi:10.1164/rccm.201707-1446LE (2018). [PubMed: 28934552]

201. Nandy S et al. Diagnostic Accuracy of Endobronchial Optical Coherence Tomography for the Microscopic Diagnosis of Usual Interstitial Pneumonia. Am J Respir Crit Care Med Online ahead of print (2021).

202. Khan SM et al. A global review of publicly available datasets for ophthalmological imaging: barriers to access, usability, and generalisability. The Lancet Digital Health 3, e51–e66 (2021). [PubMed: 33735069]

203. Thondapu V et al. High spatial endothelial shear stress gradient independently predicts site of acute coronary plaque rupture and erosion. Cardiovascular Research 117, 1974–1985 (2021). [PubMed: 32832991]

204. McGovern E et al. Optical Coherence Tomography for the Early Detection of Coronary Vascular Changes in Children and Adolescents After Cardiac Transplantation: Findings From the International Pediatric OCT Registry. JACC Cardiovasc Imaging 12, 2492–2501, doi:10.1016/j.jcmg.2018.04.025 (2019). [PubMed: 30031706]

205. Lorenser D et al. Ultrathin side-viewing needle probe for optical coherence tomography. Optics letters 36, 3894–3896 (2011). [PubMed: 21964133]

206. Boppart S, Drexler W, Morgner U, Kirtner F & Fujimoto J in Proceedings of Inter-Institute Workshop on In Vivo Optical Imaging at the National Institutes of Health. 56–61 (Citeseer).

207. Barton JK, Hoying JB & Sullivan CJ Use of microbubbles as an optical coherence tomography contrast agent. Academic radiology 9, S52–S55 (2002). [PubMed: 12019894]

208. Tucker-Schwartz J, Meyer T, Patil C, Duvall C & Skala M In vivo photothermal optical coherence tomography of gold nanorod contrast agents. Biomedical optics express 3, 2881–2895 (2012). [PubMed: 23162726]

209. Keahey P et al. Spectral-and polarization-dependent scattering of gold nanobipyramids for exogenous contrast in optical coherence tomography. Nano Letters 21, 8595–8601 (2021). [PubMed: 34644094]

210. Yang H-C et al. A dual-modality probe utilizing intravascular ultrasound and optical coherence tomography for intravascular imaging applications. IEEE transactions on ultrasonics, ferroelectrics, and frequency control 57, 2839–2843 (2010). [PubMed: 21156380]

211. Ono M et al. Advances in IVUS/OCT and future clinical perspective of novel hybrid catheter system in coronary imaging. Frontiers in cardiovascular medicine 7, 119 (2020). [PubMed: 32850981]

212. Allen WM et al. Wide-field optical coherence micro-elastography for intraoperative assessment of human breast cancer margins. Biomedical optics express 7, 4139–4153 (2016). [PubMed: 27867721]

Author Manuscript Author Manuscript Author Manuscript Author Manuscript

Box 1:

Image quality

The following key quantitative parameters of OCT system performance directly influence image quality.

Resolution

Image resolution along the optical axis is commonly referred to as axial resolution and is determined by the wavelength, λ, and spectral extent of the light source, Δλ:

$$\delta z = \frac{2\ln 2}{\pi}\frac{\lambda_0^2}{n\Delta\lambda},$$

where n is the refractive index of the sample medium. It is common to specify a system's resolution 'in air', meaning with a unitary index of refraction. Typically, OCT systems provide axial resolution between 1 μm and 10 μm.

Resolution in the plane perpendicular to the optical axis is defined in terms of the focal spot size, which is determined by the optical system f-number numerical aperture, NA. Common OCT systems provide transverse resolution of 20 – 30 μm.

Depth range

The axial range over which reflections may be detected and correctly located, referred to as depth range, is determined by the spectral resolution. In spectral domain, spectral resolution depends upon the design and alignment of the spectrometer; in frequency domain, it is determined by the instantaneous line width of the laser.

Sensitivity

Detection sensitivity is defined by the sample reflectivity that gives rise to a signal equal to the power of the system noise floor. Noise comes from quantization and electrical noise in digital electronics, thermal noise of photodiode receiver, RIN of light source (potentially attenuated by common mode rejection of receiver), and by shot noise. Optimal systems are configured so that shot noise is the dominant term. Practically, systems with −95 dB sensitivity are thought to be sufficient but typically high performance systems operate closer to −115 dB. Higher speed, resolution, or scan range may compromise sensitivity.

Roll-off:

Detection sensitivity typically is not constant over the entire depth-range. The degree to which the sensitivity diminishes through the range is referred to as roll-off, which is quantified by the range over which the sensitivity drops by 3 dB of fringe amplitude or, equivalently, 6 dB in signal intensity.

Author Manuscript Author Manuscript Author Manuscript Author Manuscript

Dynamic range:

The ratio between the maximum and minimum sample reflectivity that may be measured without modification to the system is the dynamic range. OCT systems commonly provide dynamic range in excess of 60 dB.

Author Manuscript Author Manuscript Author Manuscript Author Manuscript

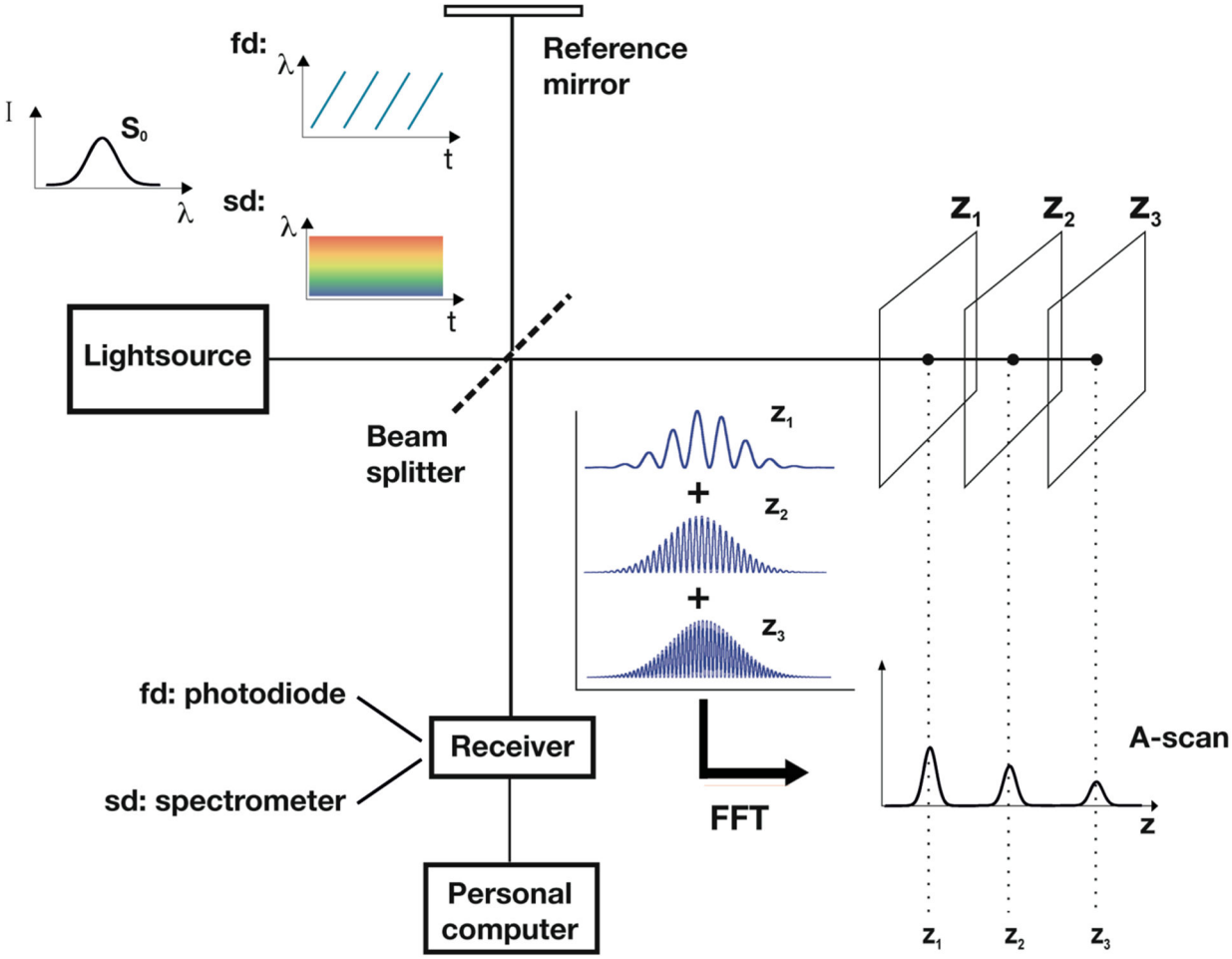

Figure 1. Basic OCT system configuration.

Temporally incoherent (multiple wavelengths) and spatially coherent light from a source is directed through an interferometer to a sample and a controlled reference path. Backreflected light is then detected and digitized. A computer is used for signal and image processing and display.

Author Manuscript Author Manuscript Author Manuscript Author Manuscript

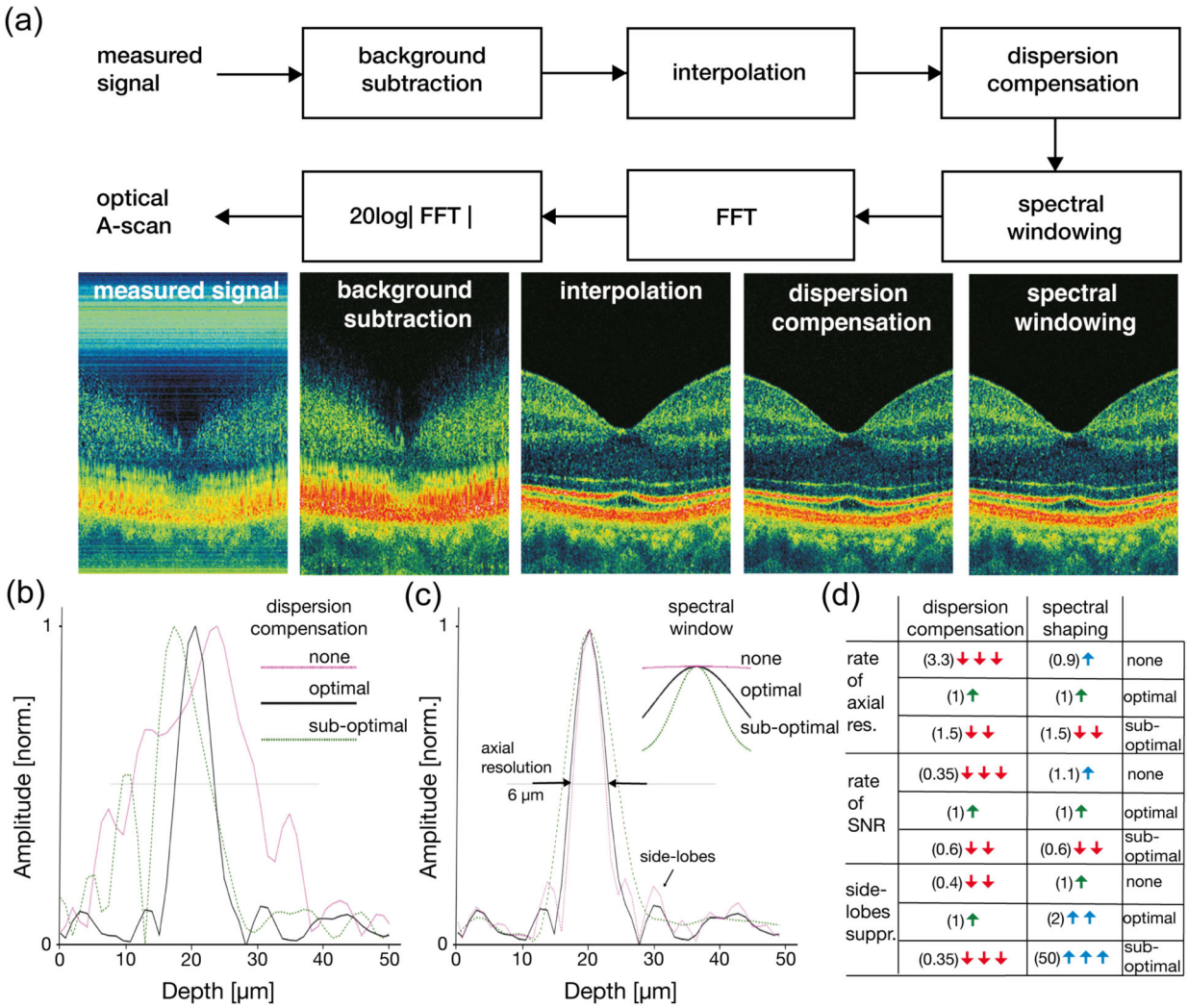

Figure 2: Basic OCT signal analysis:

(a) Block diagram Background subtraction is initially applied to the raw digital signal. Although some systems may intrinsically record the interferometric signal as a function of wavenumber (inverse wavelength), most systems require a step of interpolation to ensure equal k-sampling. Numerical compensation of any imbalance of the dispersion in the reference vs the sample interferometer path improves resolution (b). In fd-OCT systems, this step may be accompanied by compensation for any nonlinearity in the wavelength sweep of the laseUsing the optimal parameters of the correction function, it is possible to remove nonlinearities from the fringe signal and thus maximize the SNR and minimize the width of the PSF axial function - in this case, by compensating for dispersion, a 3.3-fold improvement in axial resolution is achieved (d). Application of a suboptimal correction function can result in the appearance of asymmetry, large side-lobs and PSF broadening even with small mismatches of this function (green dashed line) (d). A spectral window, typically a Gaussian or Hamming filter, is applied to control the shape of the axial point spread function (c)When the window (in this case Gaussian) is used optimally, a reduction in side-lobs is achieved at the expense of a broadening of the PSF and a loss of axial

Author Manuscript Author Manuscript Author Manuscript Author Manuscript

resolution (d). When a suboptimal window (narrower than the original spectrum) is used, removal of side-lobs is associated with a significant loss of axial resolution and SNR (d). Conversion of the fringe data to reflectance as a function of depth is performed using Fourier transformation. The large dynamic range of OCT data is preserved for display using logarithmic compression to form the final axial reflectance profile or ‘A-line’.

Author Manuscript Author Manuscript Author Manuscript Author Manuscript

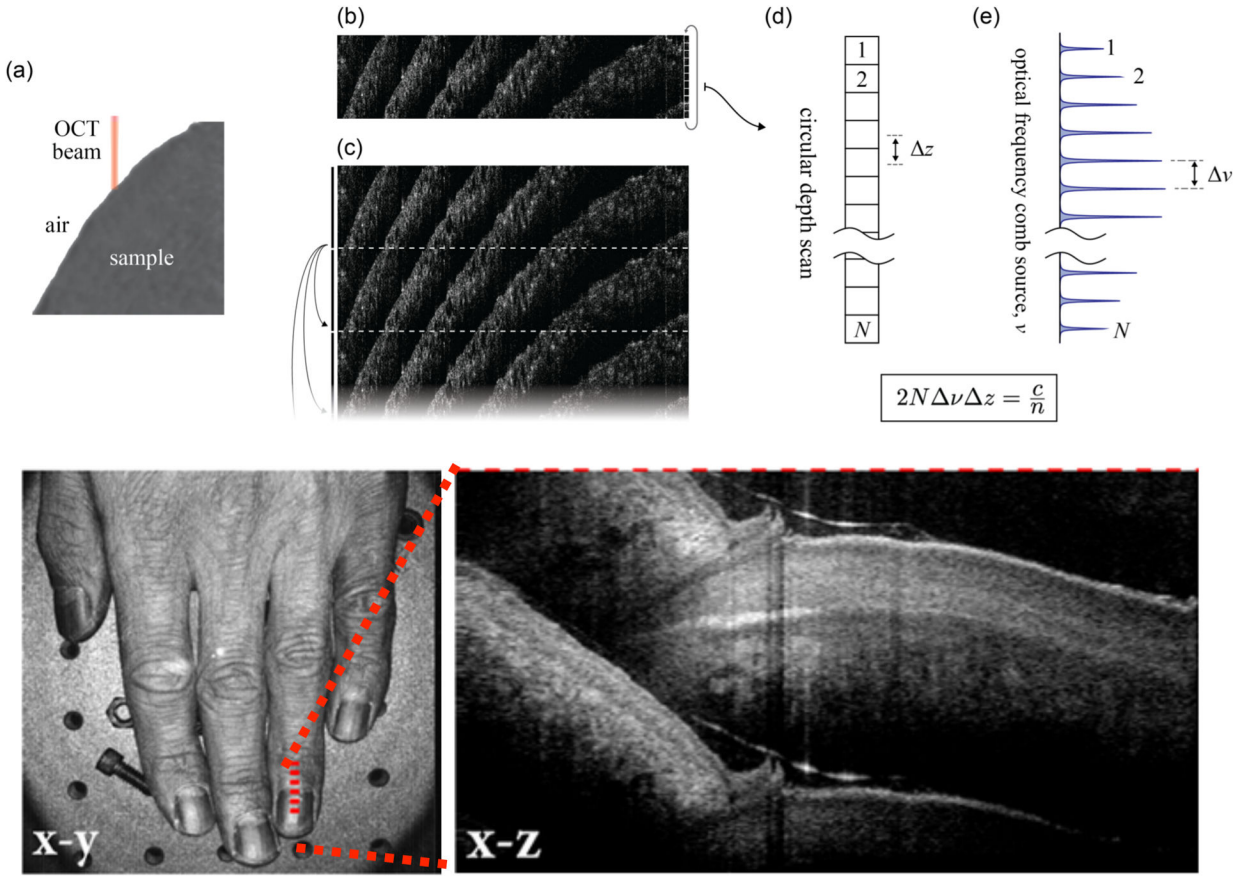

Figure 3: Circular ranging concept.

The imaging properties of a CR-OCT. a. When conventional OCT is used to image a sample with a large variation in height, a significant portion of the measurement data describes “empty” space, which are the regions above the sample surface and beyond the imaging penetration depth. b. A CR-OCT image collects multiple depth locations into each measurement such that the sample appears as though it had been circularly wrapped onto itself. Because this wrapped image is a more data compact representation of the sample, it can be captured with fewer measurements. c. The upper and lower image boundaries of CR-OCT images are cuts through a continuous circular delay. This can be seen by noting the continuity of the sample when these images are tiled vertically. d. An A-line in the CR image describes the sample as a function of a looped circular depth coordinate. This depth spacing between measurements (Δz) and number of depth pixels (N) in the depth A-line are directly related to the combline spacing (Δz) and the number of comblines (N) in the optical frequency comb source used to perform CR-OCT imaging. An image of a human hand atop an optical table is depicted in the lower left panel as an x-y (transverse) projection. At any every point in this image, it is possible to display the corresponding cross-sectional image. One cross-sectional image, across the nail-fold region of the left ring finger, demonstrates the depth of penetration and resolution characteristic of state-of-the-art conventional OCT.

Author Manuscript Author Manuscript Author Manuscript Author Manuscript

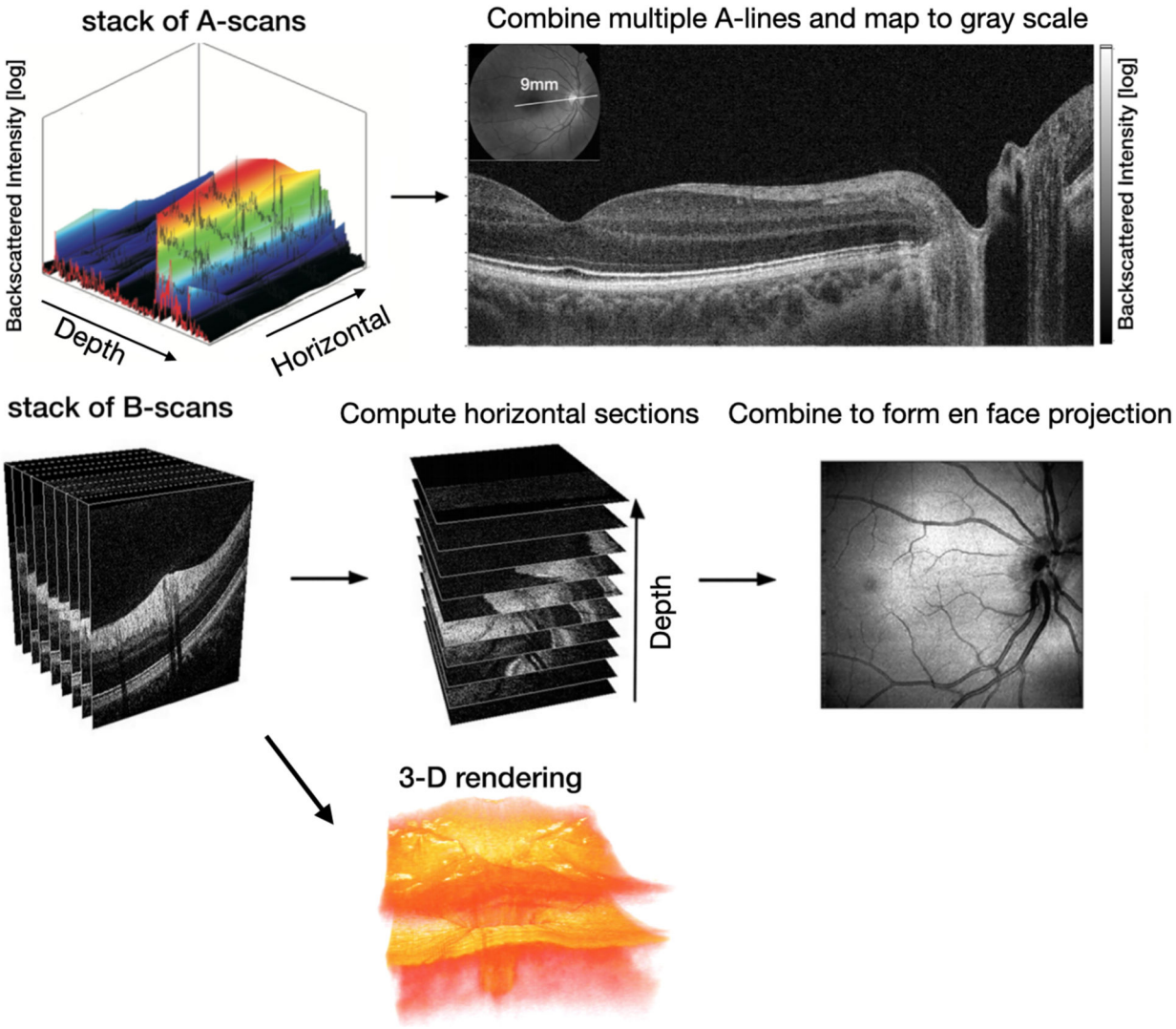

Figure 4: Basic image processing steps.

Multiple A-line (depth, z) scans are acquired while the OCT beam is swept transversally across the sample. Cross-sectional (transverse - depth) images (B-scans) are computed by combining multiple A-lines and mapping the reflectance data to gray scale. Typically images are displayed with isotropic scale. Data corresponding to multiple B-scans may be acquired with a second direction of transverse scanning (x-y). The resulting data volume may be processed to compute horizontal sections or en-face projections. In some cases, three-dimensional visualization of the data may assist interpretation and further extraction of sub-volume of interest. In the case of rotational catheter scanning systems, the typical acquisition coordinates are cylindrical: r (depth) and θ-z (transverse).

Author Manuscript Author Manuscript Author Manuscript Author Manuscript

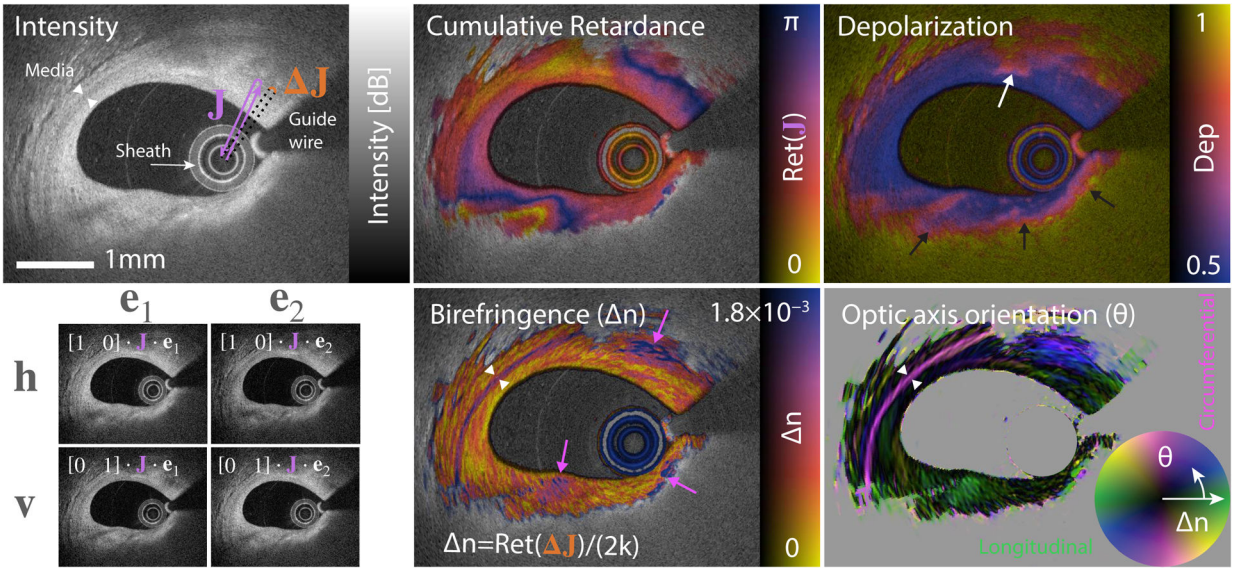

Figure 5: Polarization-sensitive OCT results.

Catheter-based PS-OCT in the left circumflex coronary artery of a 52-year-old male patient undergoing percutaneous coronary intervention. Polarization-diversity detects the signal along two linear orthogonal polarization states (h,v) in response to illumination by two input polarization states (e1, e2) (bottom left). The incoherent mean of all signals serves to visualize the conventional scattering signal of OCT (top left). The retardance of the round-trip Jones matrix (J) demonstrates tissue anisotropy but is difficult to interpret because it cumulates the effect of propagation through tissue layers (top middle). In comparison, analysis of the local Jones matrix reveals depth-resolved tissue birefringence (Δn, bottom middle) and optic axis orientation (θ, bottom right) and clearly delineates tissue layers (media, white arrow heads) with distinct anisotropy (purple arrows point to areas with increased Δn), suggestive of increased collagen and smooth muscle cell content or cholesterol crystals. Depolarization, computed using the incoherent Mueller-Stokes formalism quantifies the randomization of the detected polarization states, caused by scattering in lipid-rich plaques and macrophages, or by the absence of meaningful signal. Scale bar: 1 mm.

Author Manuscript Author Manuscript Author Manuscript Author Manuscript

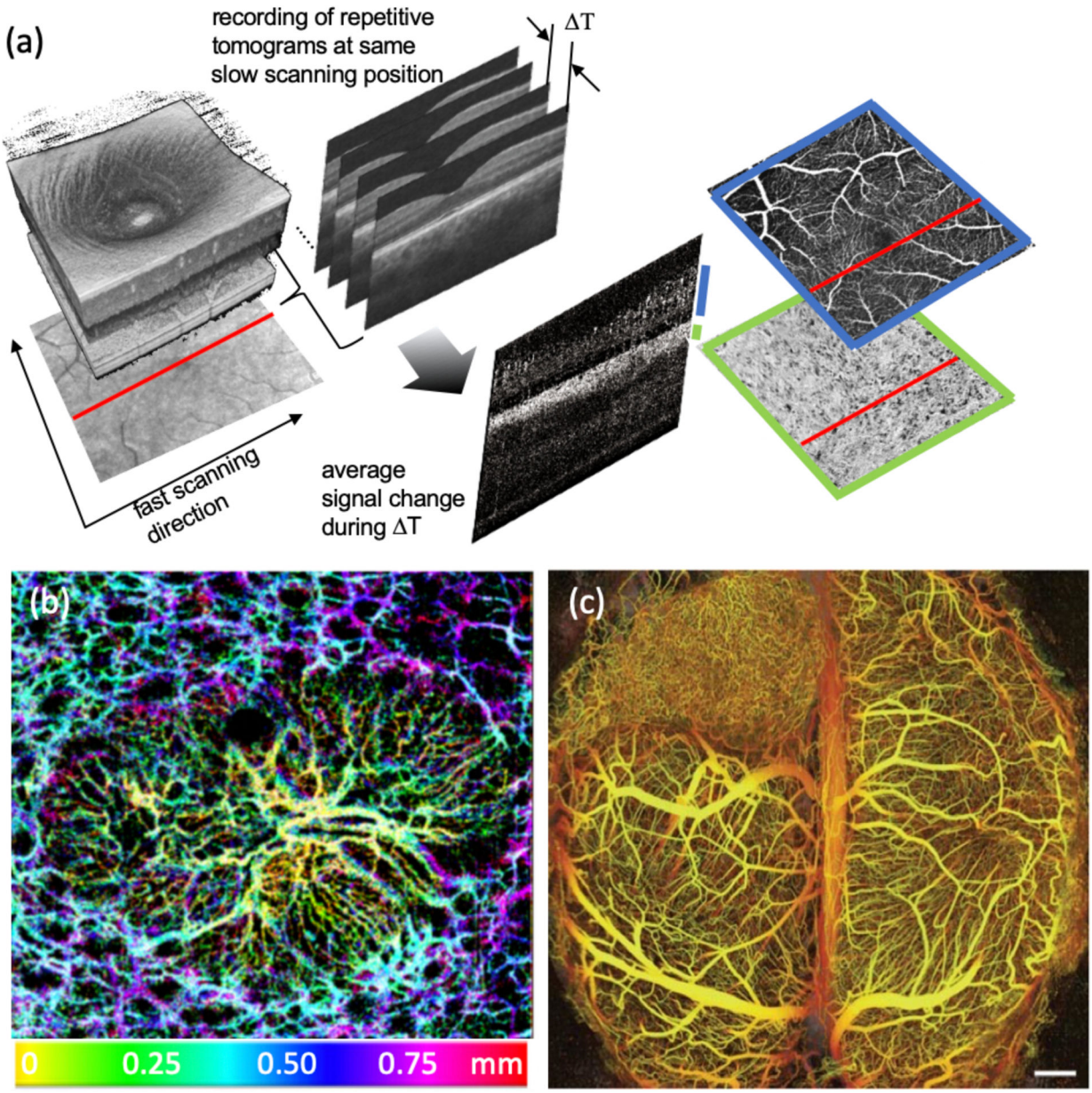

Figure 6: OCT Angiography principle and results.

Steps to calculate OCTA enface maps starting from series of tomograms taken at the same slow scanning position at time intervals ΔT to enface projection views at indicated depth ranges (a); nodular basal cell carcinoma in skin, the color coded depth ranges are indicated in the color bar(reproduced from[127] (b). OCTA of a xenotransplanted U87 human glioblastoma multiforme tumor in a mouse brain. Depth-projected vasculature within the first 2 mm is color coded by depth, ranging from yellow (superficial) to red (deep). Scale bar, 500 μm (c) (reproduced from[24]);

Author Manuscript Author Manuscript Author Manuscript Author Manuscript

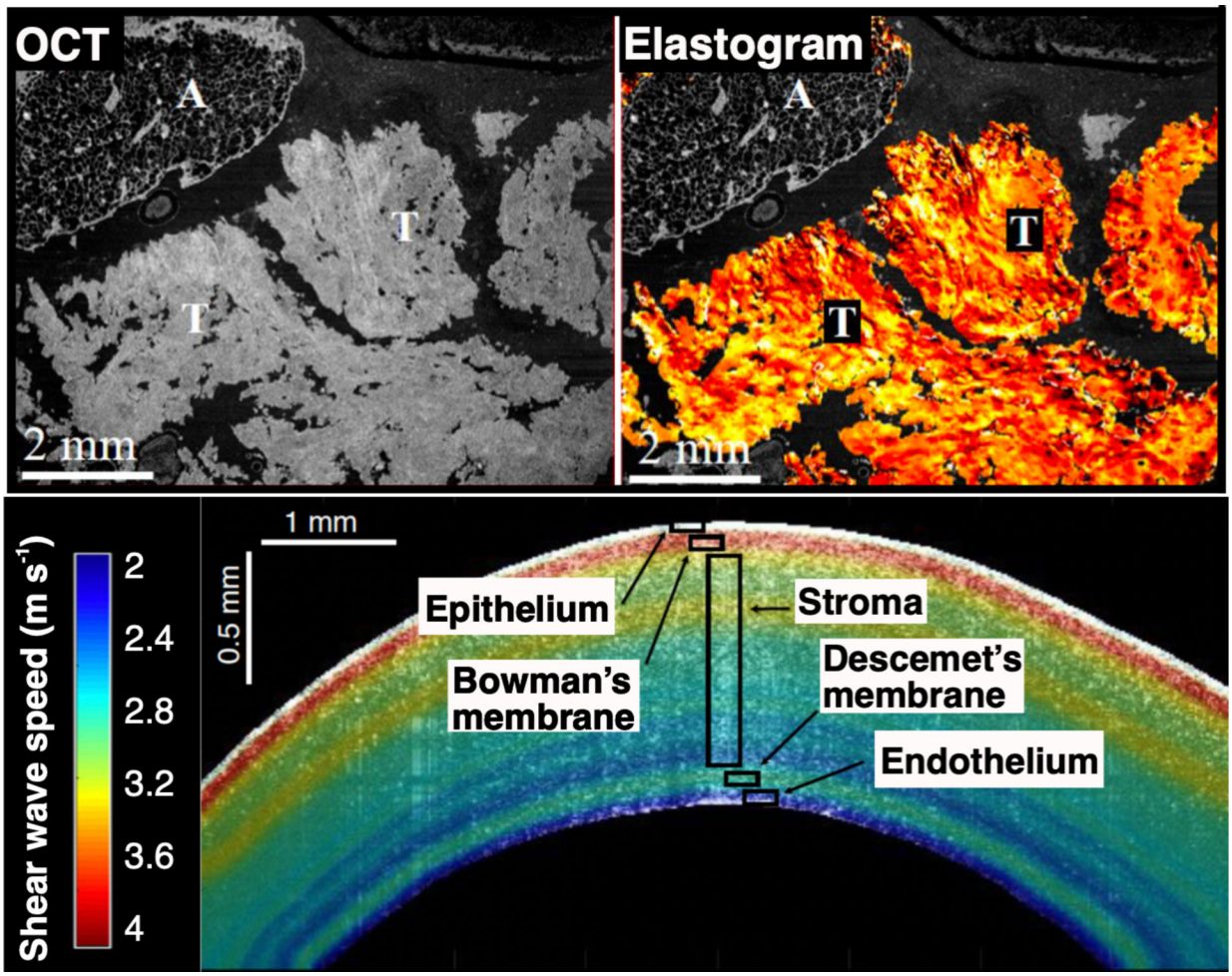

Figure 7: Elastography results.

OCT intensity image and corresponding elastogram (upper panels) of human breast tissue (reproduced in part from [212]. Elevated stiffness of tumor is readily detected by elastographic OCT. Measurements of shear wave speed (lower panel) provide for the identification of important structural layers within the human cornea. [Reproduced in part from [86]]

Author Manuscript Author Manuscript Author Manuscript Author Manuscript

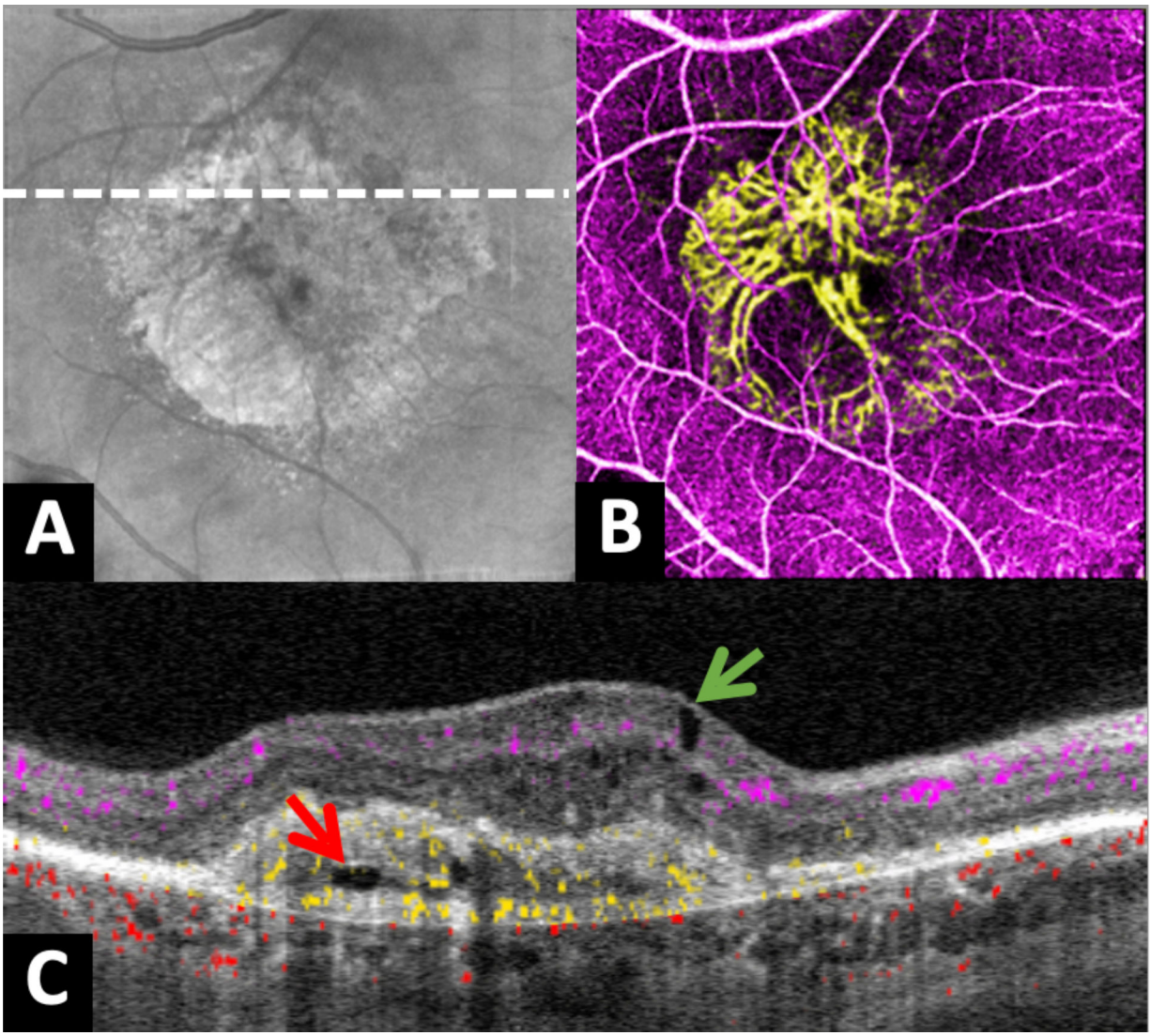

Figure 8: Ophthalmic application.

An eye with exudative age-related macular degeneration. (A) En face structural OCT. The dotted line transects the cross section shown in panel C. (B) En face OCT angiogram with color coded flow signal (inner retina in violet and outer retina in yellow). The choroidal neovascularization is in the outer retina. (C) Cross-sectional projection-resolved OCT angiogram with reflectance shown in gray scale and flow signal color coded by depth (choroid in red). The neovascular membrane is in the outer retina (yellow) under the pigment epithelium. Intraretinal cyst (green arrow) and subretinal fluid (red arrow) are indications for an anti-neovascular injection.

Author Manuscript Author Manuscript Author Manuscript Author Manuscript

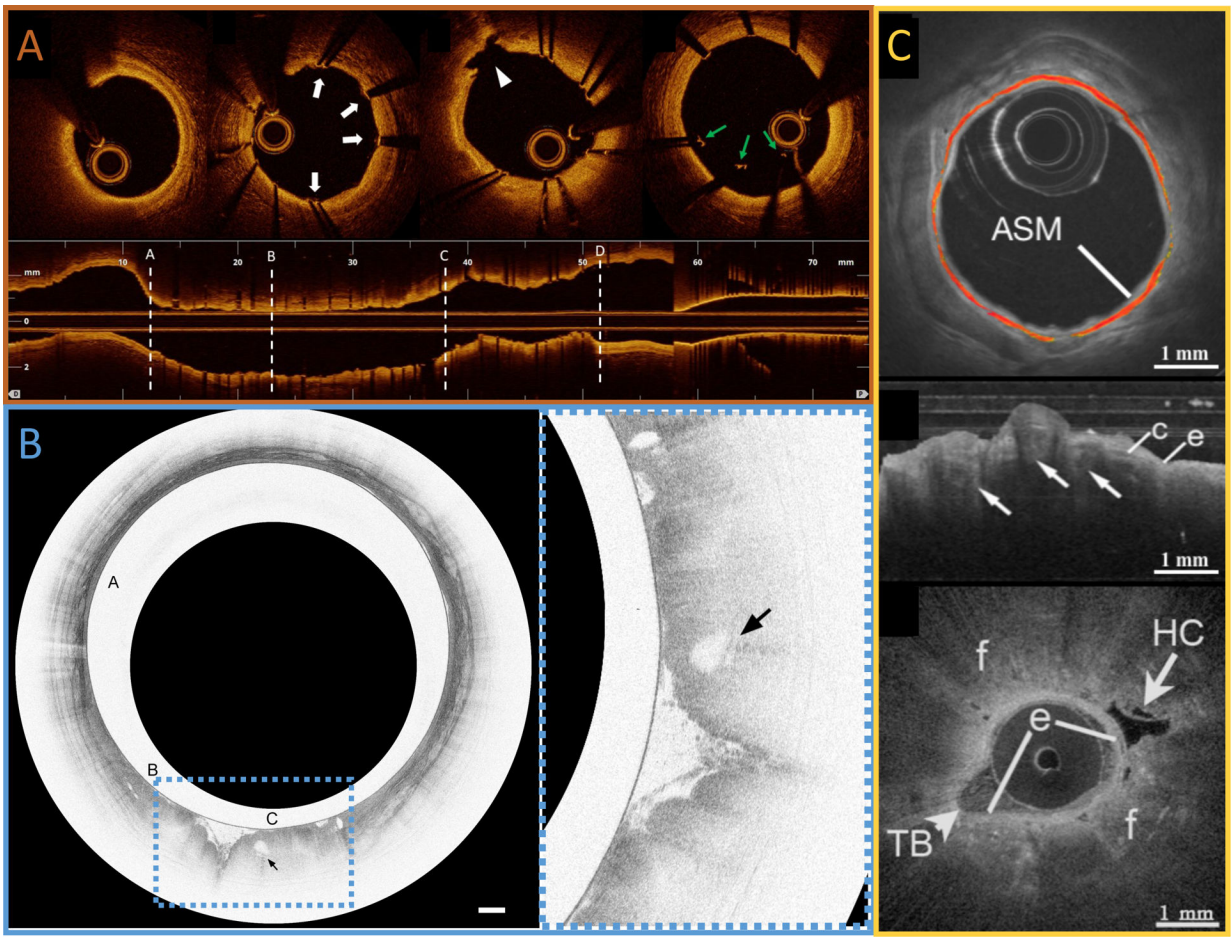

Figure 9: Catheter and endoscopic applications.

Figure 9a Representative fd-OCT images of the coronary artery after stent implantation. Upper panel shows cross sectional images and lower panel longitudinal pull-back image. Based on the baseline OCT measurements before PCI showing 2.6mm and 3.4mm lumen diameters at distal and proximal reference sites, respectively, with the lesion length of 31.8mm, the operator implanted a stent with a 3.0mm diameter and 38mm length. A lipid-laden atheroma (5 – 12 o'clock) is observed distal to the stent (A). Struts of metallic stent are identified as reflections accompanied by back shadows (white arrows, B). Minor dissection of intima is detected between stent struts (white arrowhead, C). Significant malapposition of stent struts are visualized at the proximal edge of the stent (green arrows, D).

Figure 9b: Representative frame of a volumetric laser endomicroscopy (fd-OCT) scan performed on a patient with Barrett's esophagus with high-grade dysplasia. (A) Normal squamous epithelium demonstrates a layered architecture that transitions into Barrett's epithelium (B) characterized by effacement of the layered architecture and irregular surface. Area of Barrett's esophagus with highgrade dysplasia (C) characterized by high-surface signal intensity and dilated, irregular epithelial gland (arrow). Scale bar = 1 cm.

Figure 9c: Endobronchial fd-OCT images of pulmonary diseases, including asthma, lung cancer and interstitial lung disease. (A) Cross sectional OCT image acquired in vivo from an

Author Manuscript Author Manuscript Author Manuscript Author Manuscript

individual with mild allergic asthma. The airway smooth muscle (ASM) highlighted in red was segmented utilizing circumferentially oriented optic axis information from PS-OCT. (B) A longitudinal reconstruction of squamous cell carcinoma obtained using EB-OCT. Arrows point to squamous nests located within the tumor mass. e - epithelium, c - cartilage. (C) EB-OCT image obtained from a patient with IPF highlighting the presence of honeycombing (HC), fibrosis (f) and traction bronchiectasis (TB). Scale bars = 1mm.